Electronic Supplementary Material (ESI) for Polymer Chemistry.
This journal is © The Royal Society of Chemistry 2023

Supplementary information

A combined computational and experimental study of metathesis and nucleophile-mediated exchange mechanisms in boronic ester-containing vitrimers

Jacopo Teotonico,[a] Daniele Mantione,[a,b] Laura Ballester-Bayarri,[a] Marta Ximenis,[a] Haritz Sardon,[a,c] Nicholas Ballard[a,b] and Fernando Ruipérez[a,c]**

[a] POLYMAT, University of the Basque Country UPV/EHU, Joxe Mari Korta zentroa, Tolosa Hiribidea 72, 20018 Donostia-San Sebastián, Spain

[b] Ikerbasque, Basque Foundation for Science, 48013 Bilbao, Spain

[c] Department of Polymers and Advanced Materials: Physics, Chemistry and Technology, Faculty of Chemistry, University of the Basque Country UPV/EHU, Donostia-San Sebastián 20018, Spain

[d] Physical Chemistry Department, Faculty of Pharmacy, University of the Basque Country UPV/EHU, 01006 Vitoria-Gasteiz, Spain

*Corresponding author: E-mail address: nicholas.ballard@polymat.eu (N. Ballard), fernando.ruiperez@ehu.eus (F. Ruipérez)

Table of contents

Part-I. Characterization of model compounds, monomers, and crosslinkers

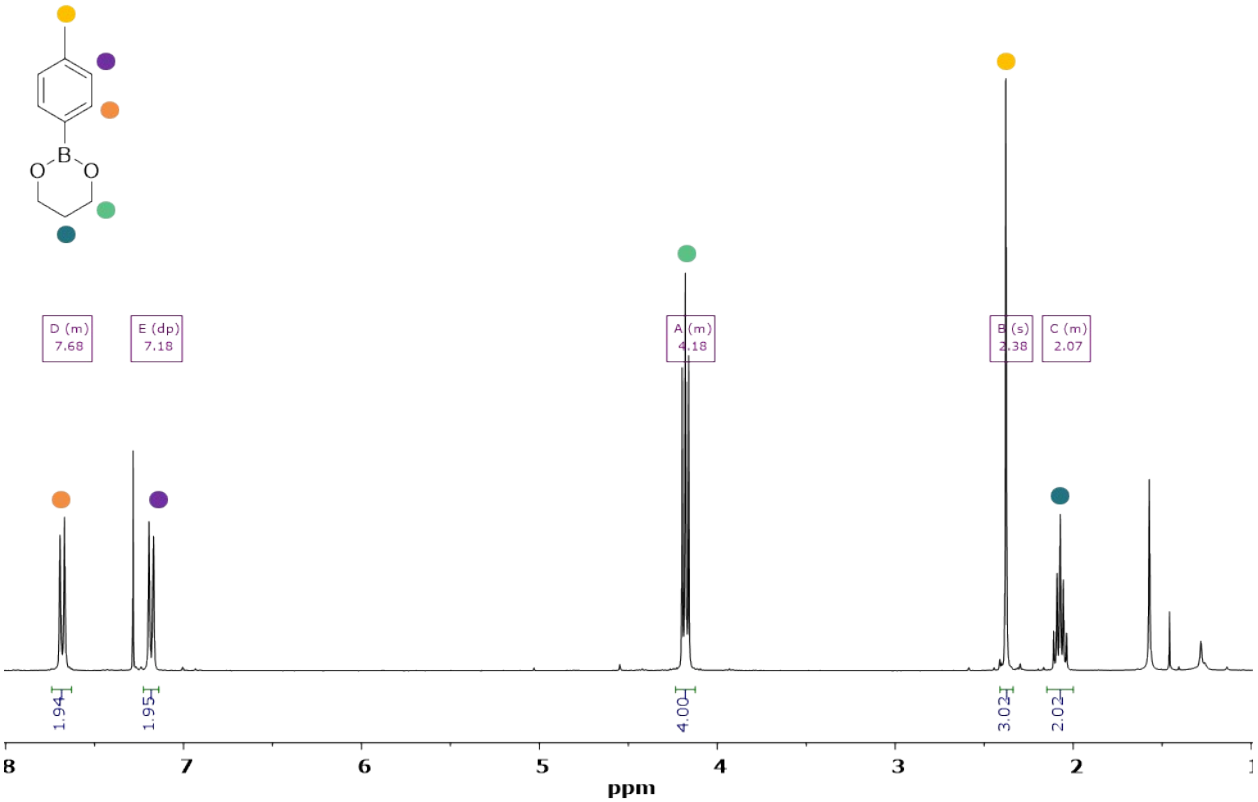

Figure S1: ^{1}H NMR of 2-(4-methylphenyl)-1,3,2-dioxaborinane (B1) in $CDCl_3$

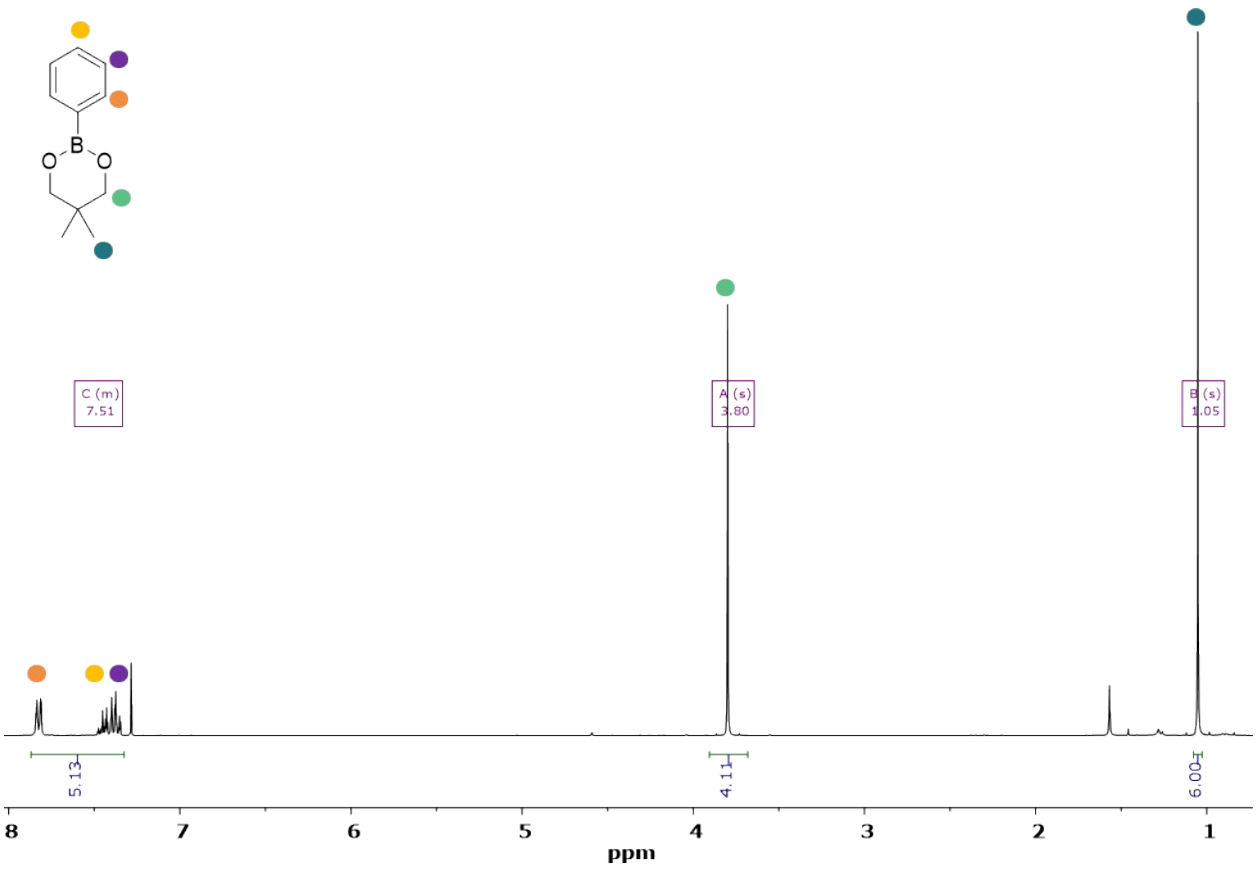

Figure S2: ^{1}H NMR of 5,5-dimethyl-2-phenyl-1,3,2-dioxaborinane (B2) in $CDCl_3$

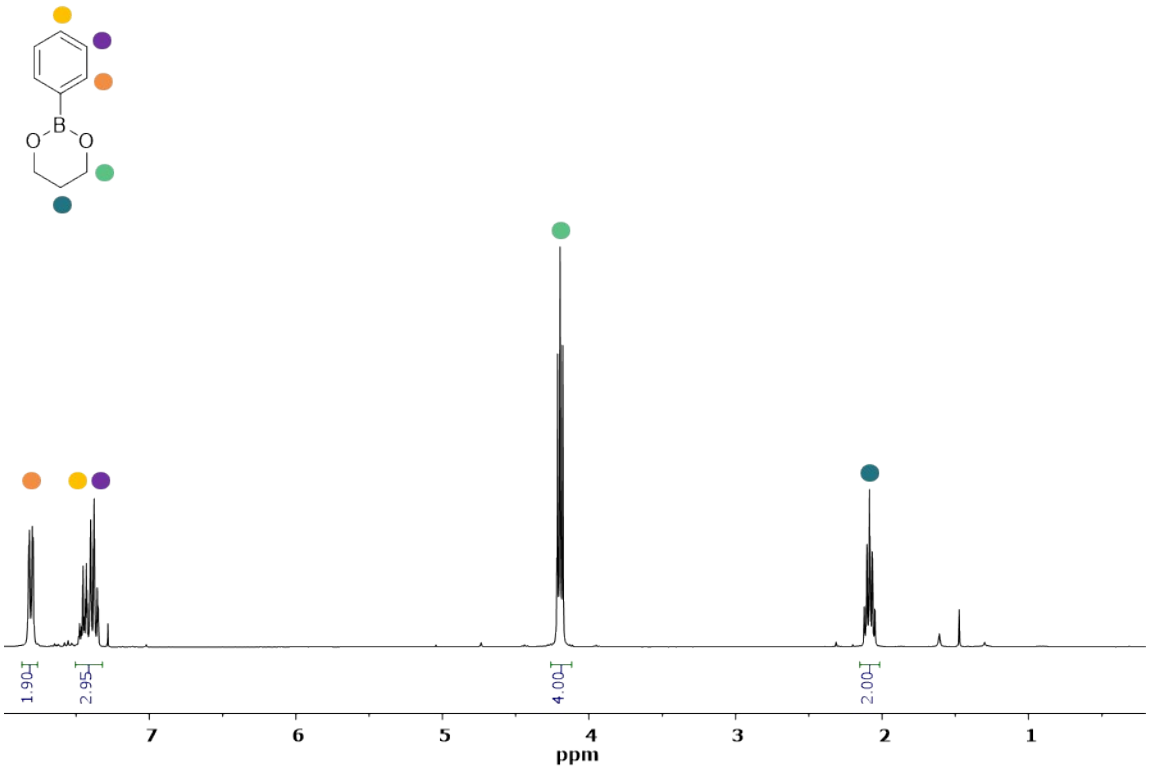

Figure S3: ^{1}H NMR of 2-Phenyl-1,3,2-dioxaborinane (B3) in $CDCl_3$

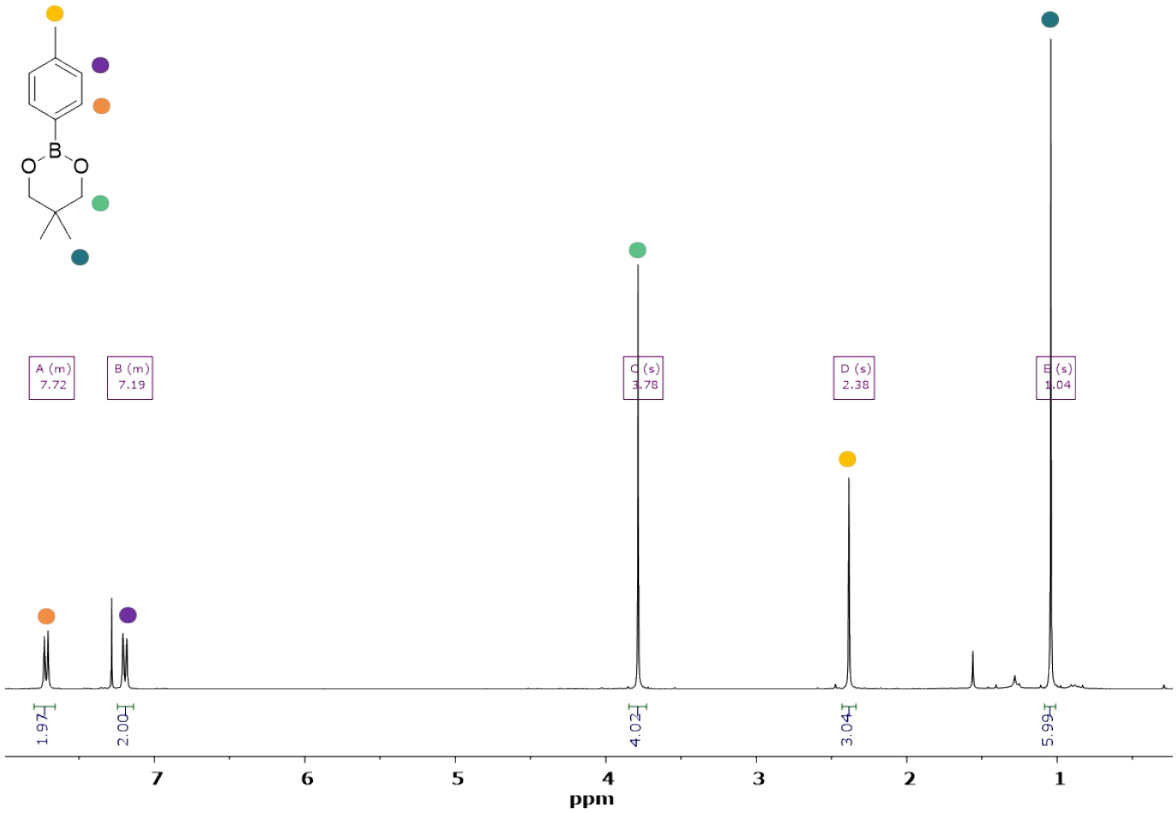

Figure S4: ^{1}H NMR of 5,5-dimethyl-2-(4-methylphenyl)-1,3,2-dioxaborinane (B4) in $CDCl_3$

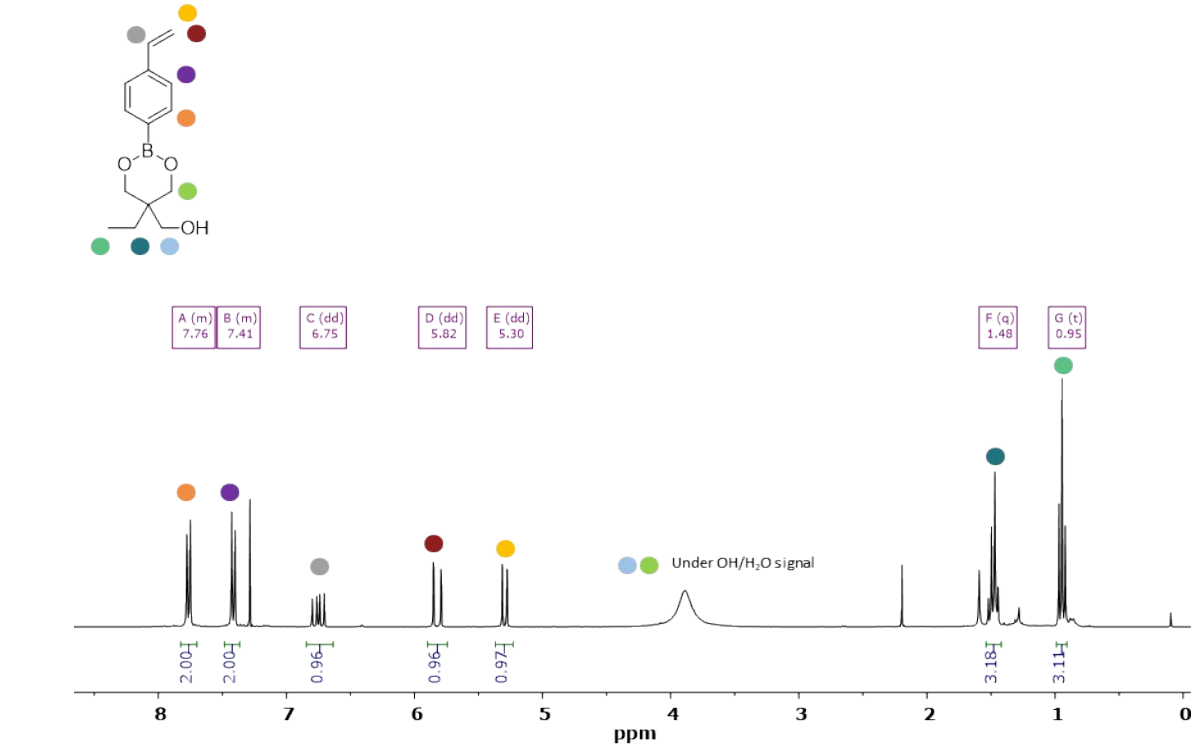

Figure S5: ^{1}H NMR of (5-ethyl-2-(4-vinylphenyl)-1,3,2-dioxaborinan-5-yl)methanol (B5) in $CDCl_3$

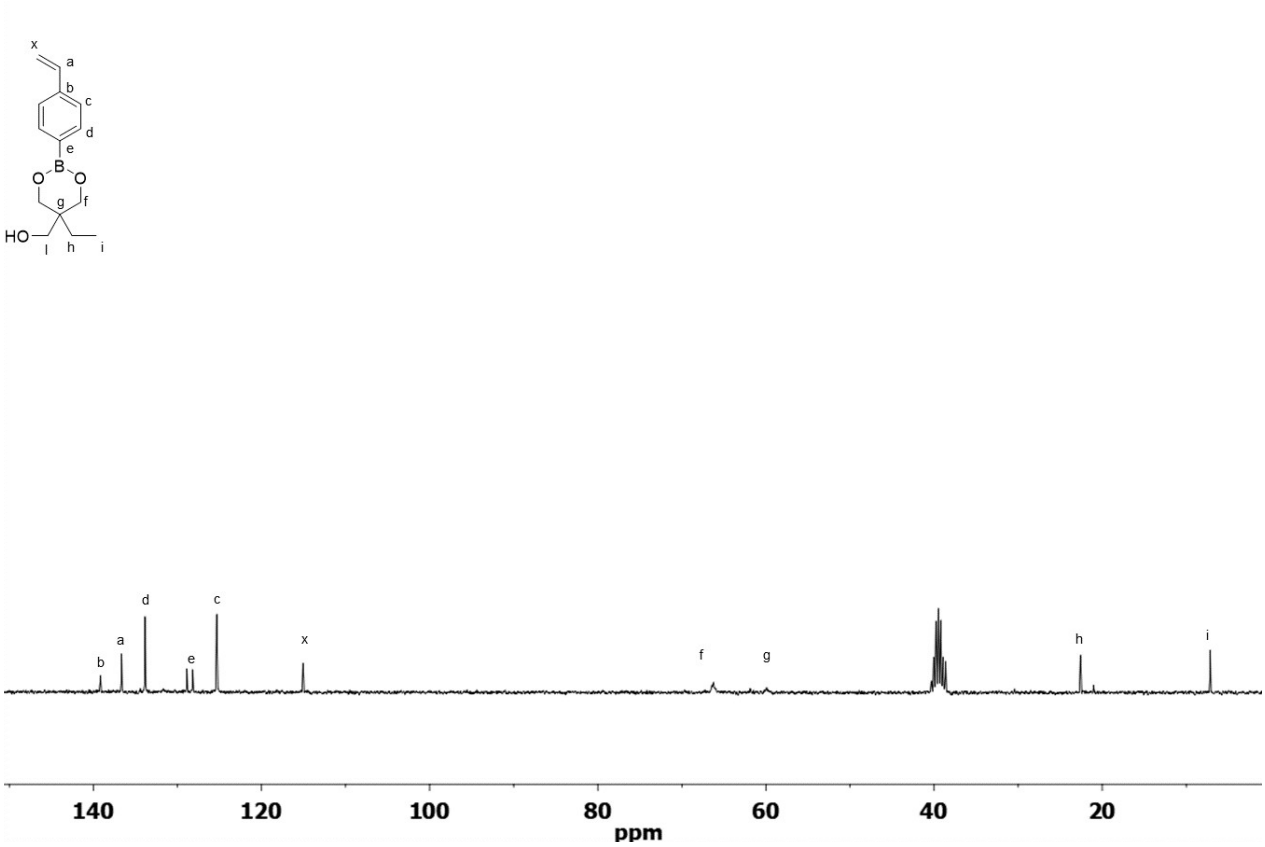

Figure S6: ^{13}C NMR of (5-ethyl-2-(4-vinylphenyl)-1,3,2-dioxaborinan-5-yl)methanol (B5) in DMSO-d^6

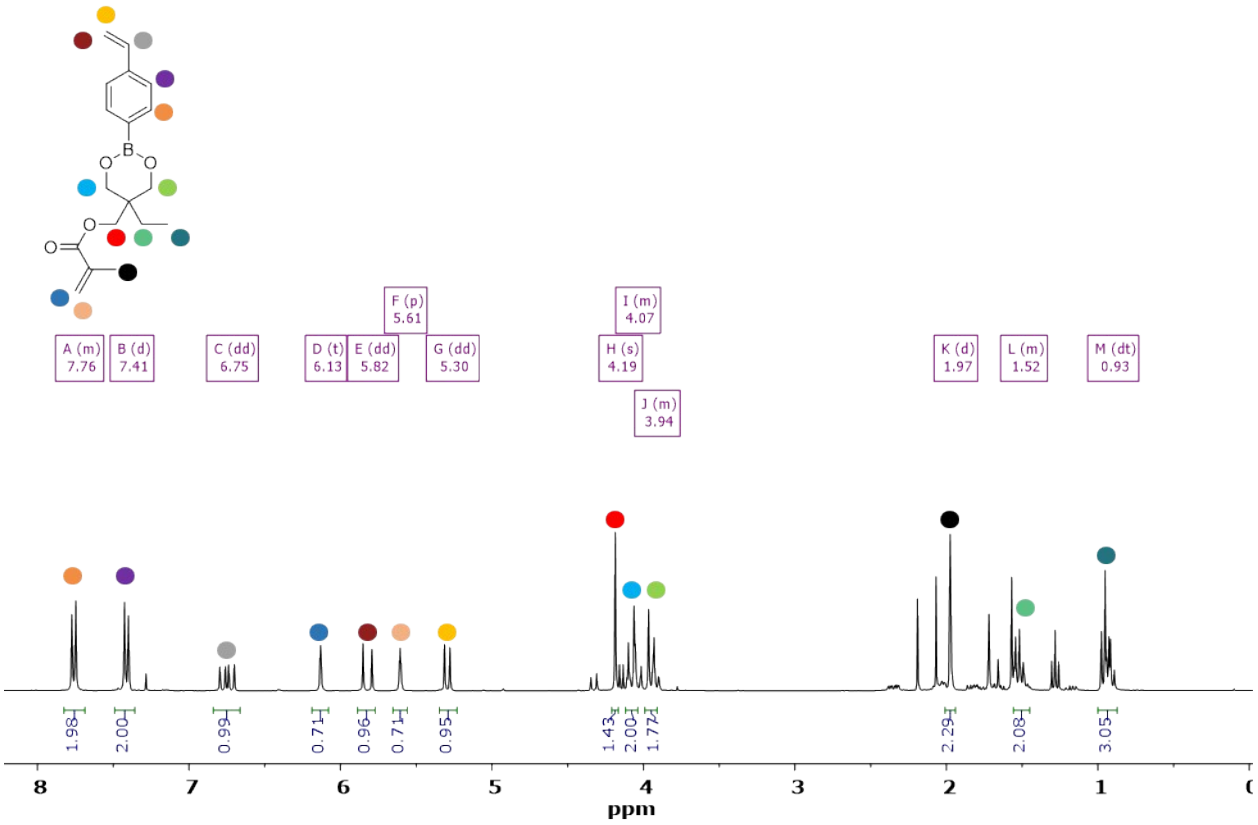

Figure S7: ^{1}H NMR of (5-ethyl-2-(4-vinylphenyl)-1,3,2-dioxaborinan-5-yl)methyl methacrylate (B6) in $CDCl_3$

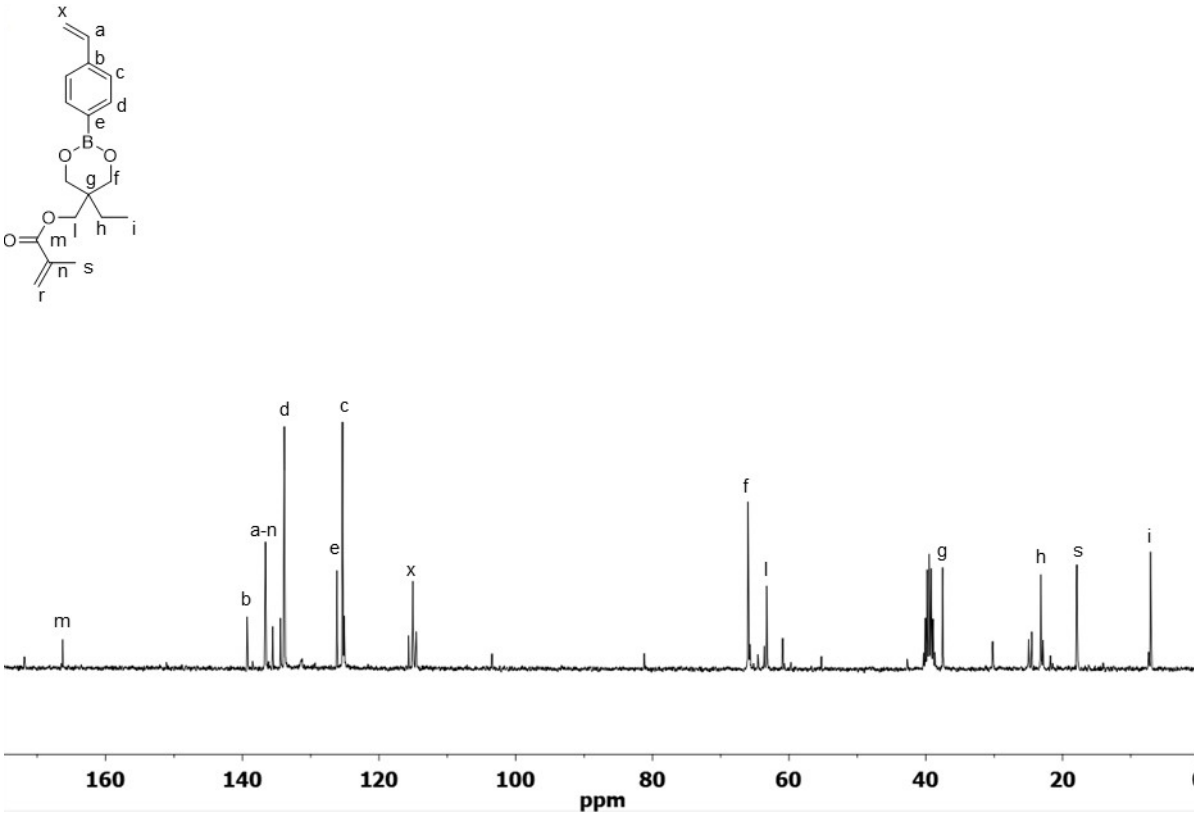

Figure S8: ^{13}C NMR of (5-ethyl-2-(4-vinylphenyl)-1,3,2-dioxaborinan-5-yl)methyl methacrylate (B6) in DMSO-d^{6}

Part-II. Kinetic and hydrolytic stability studies of model compounds

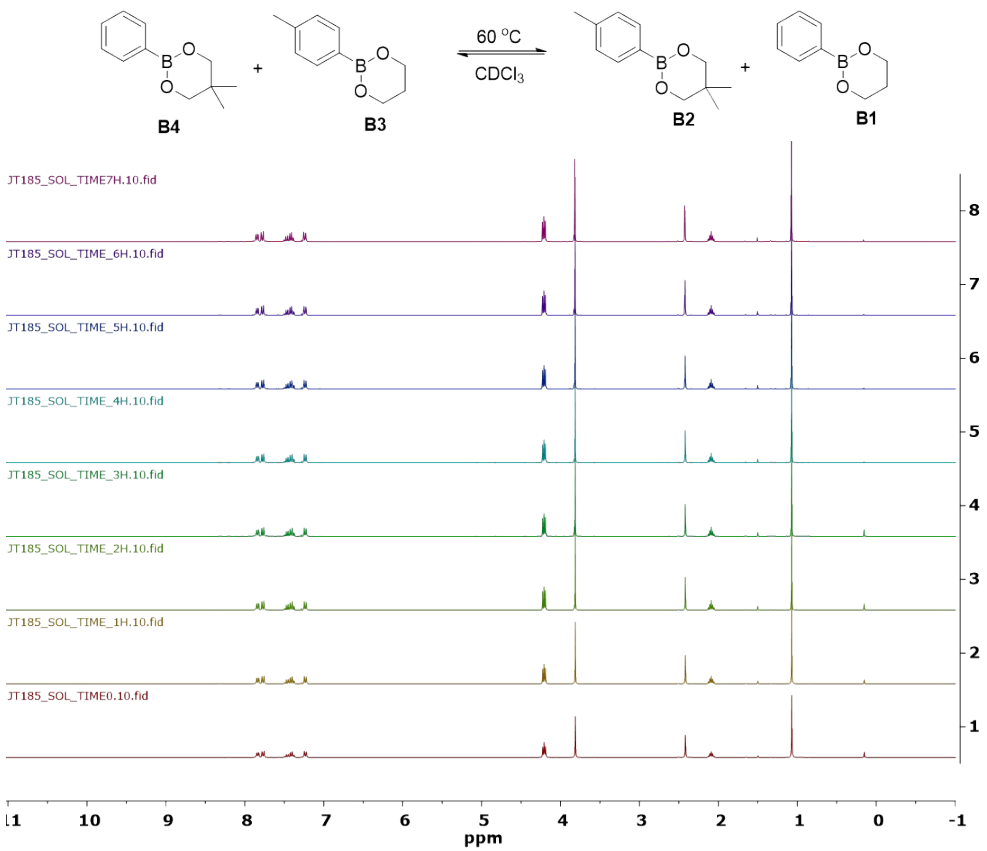

Fig. S9: Time-dependent ^{1}H NMR spectra of the reaction mixture of B4 and B3 in $CDCl_3$ at 60°C

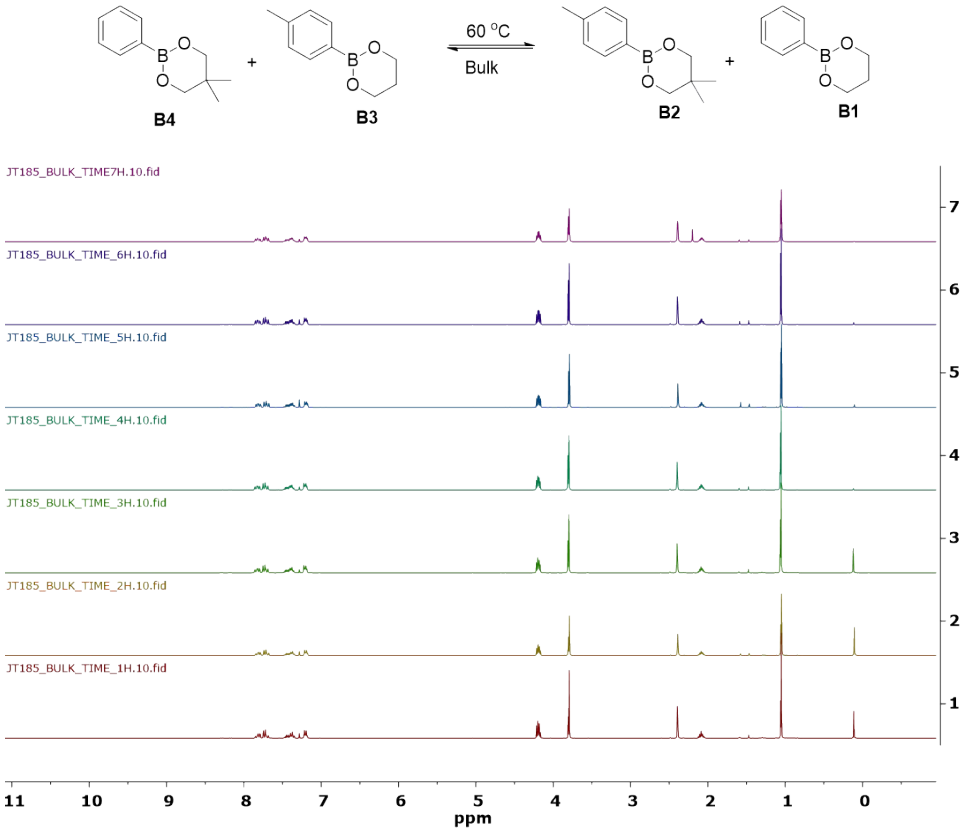

Fig. S10: Time-dependent ^{1}H NMR spectra of the reaction mixture of B4 and B3 in bulk at 60°C

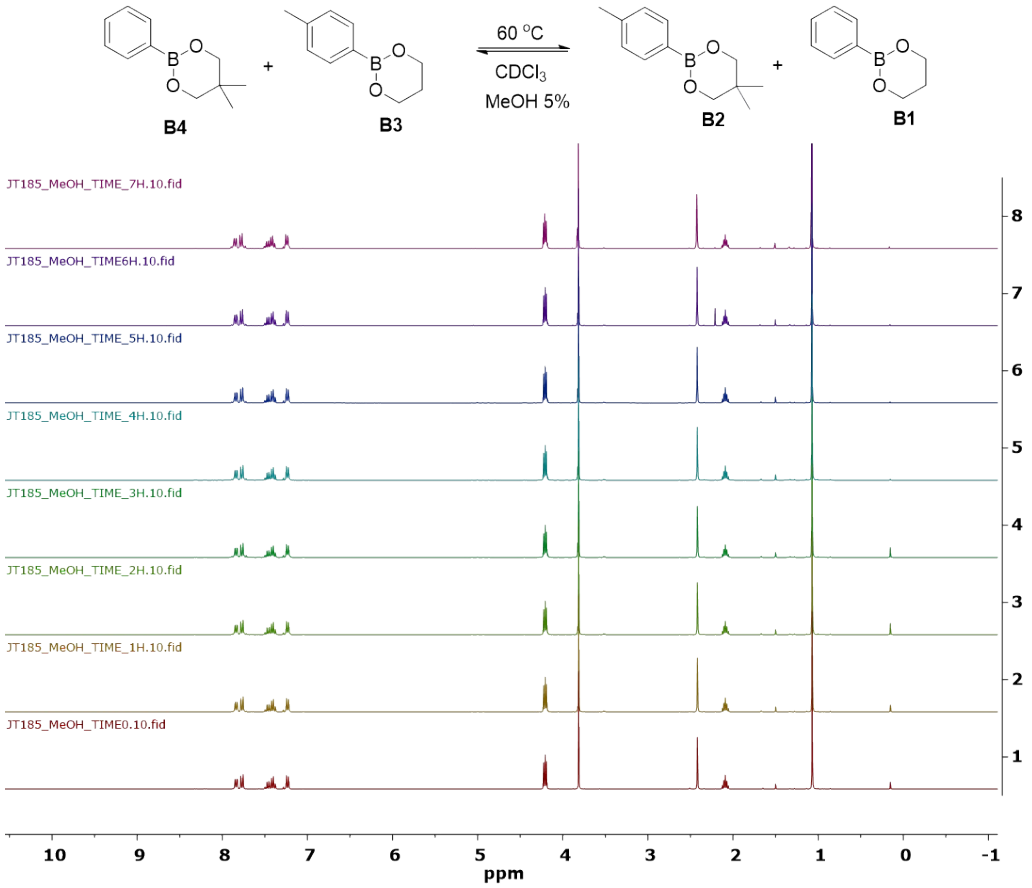

Fig. 11: Time-dependent ^{1}H NMR spectra of the reaction mixture of B4 and B3 with 5 mol% of MeOH in $CDCl_3$ at 60°C

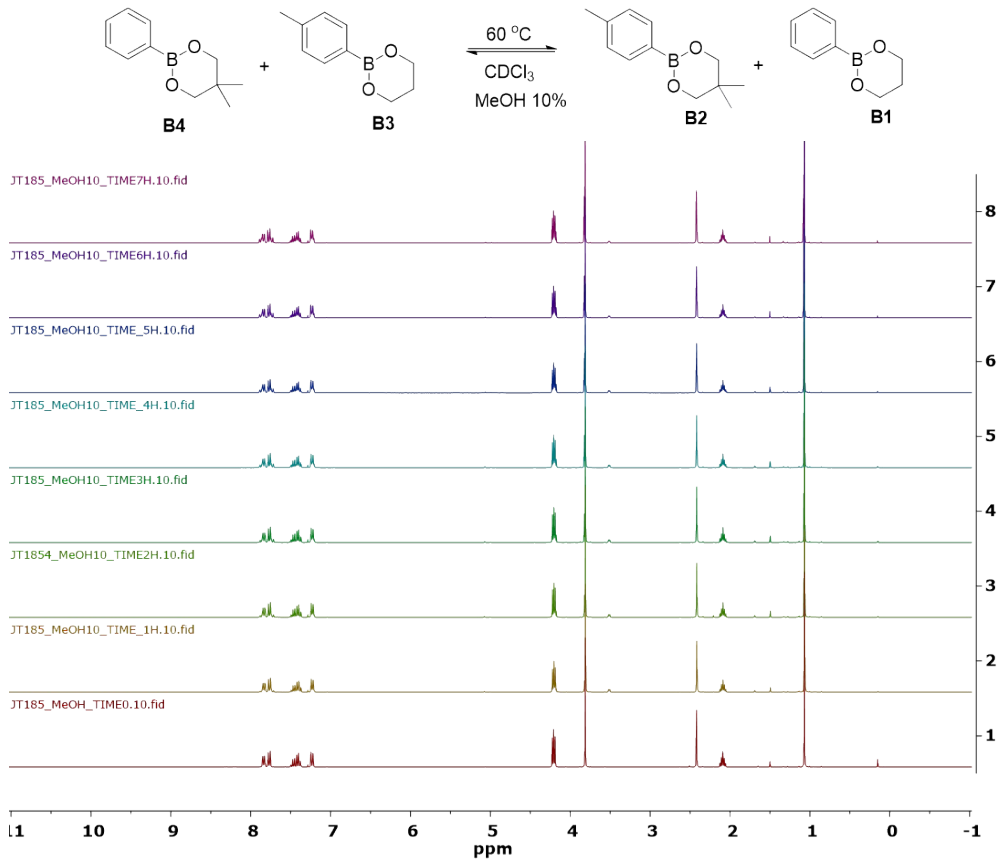

Fig. S12: Time-dependent ^{1}H NMR spectra of the reaction mixture of B4 and B3 with 10 mol% of MeOH in $CDCl_3$ at 60˚C

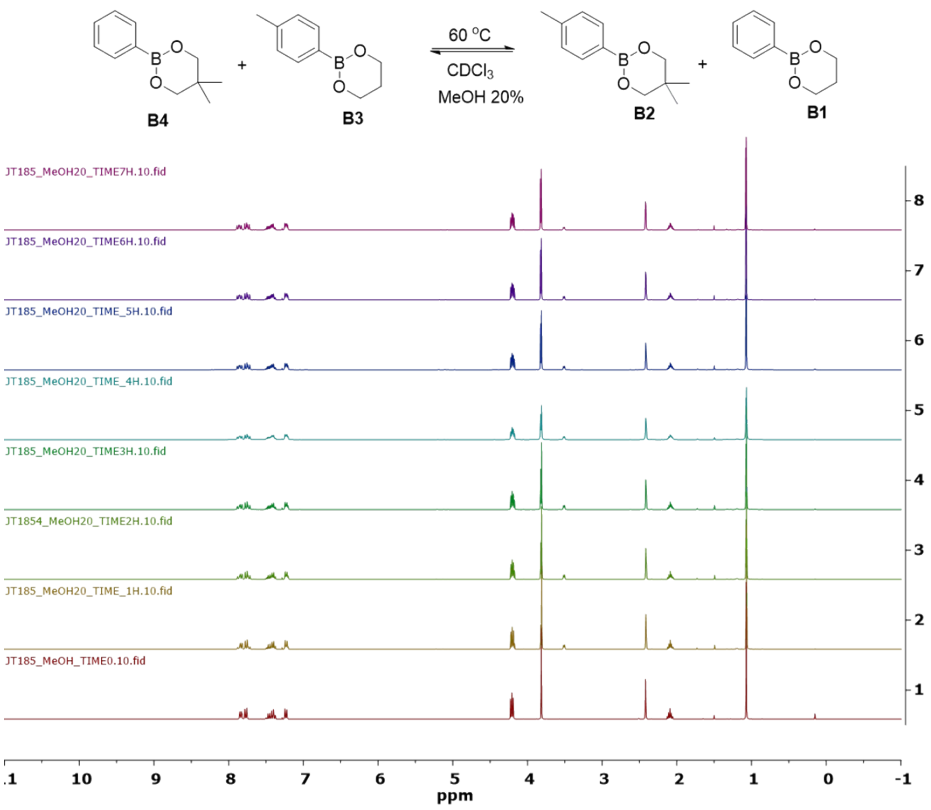

Fig. S13: Time-dependent ^{1}H NMR spectra of the reaction mixture of B4 and B3 with 20 mol% of MeOH in $CDCl_3$ at 60˚C

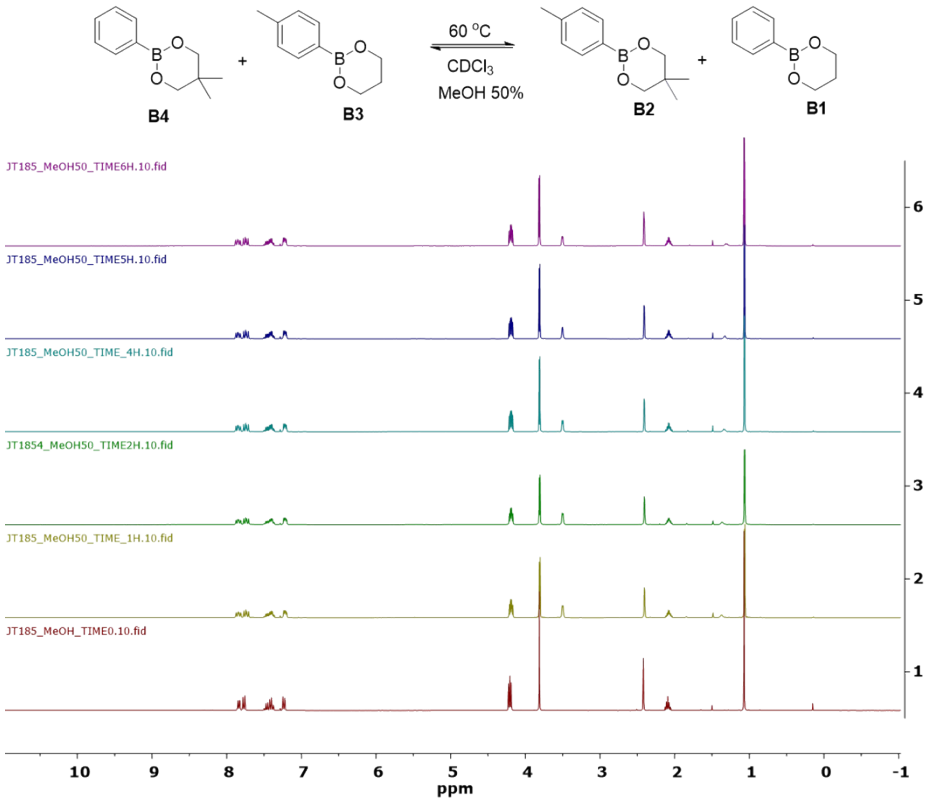

Fig. S14: Time-dependent ^{1}H NMR spectra of the reaction mixture of B4 and B3 with 50 mol% of MeOH in $CDCl_3$ at 60˚C

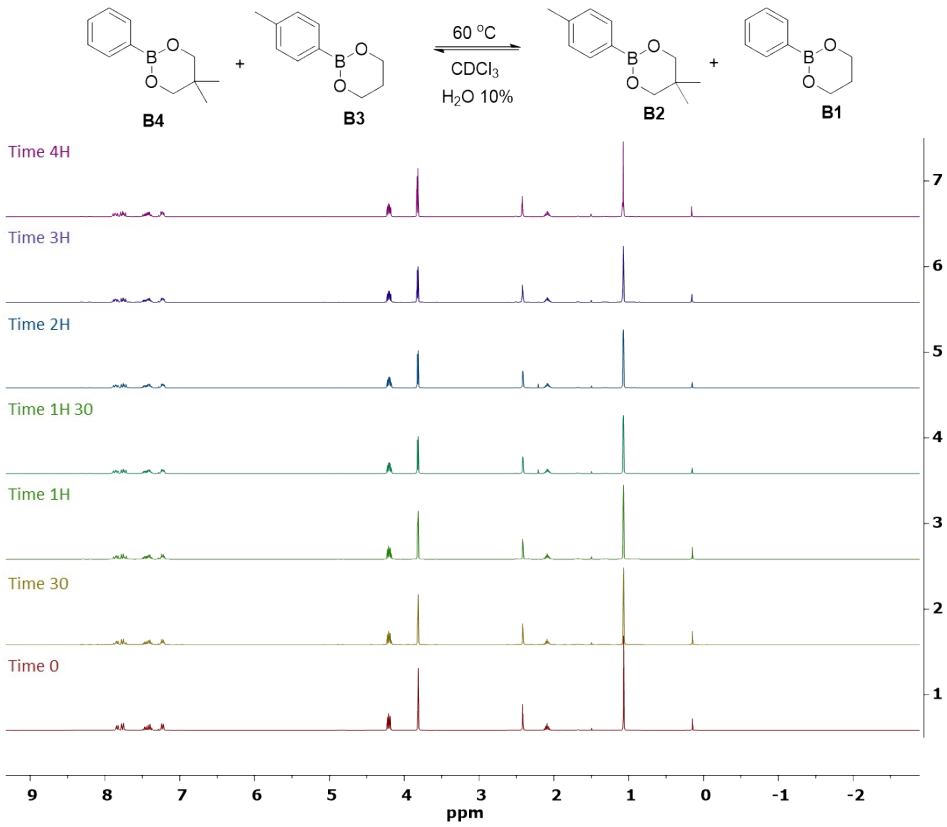

Fig. S15: Time-dependent ^{1}H NMR spectra of the reaction mixture of B4 and B3 with 10 mol% of H_2O in $CDCl_3$ at 60˚C

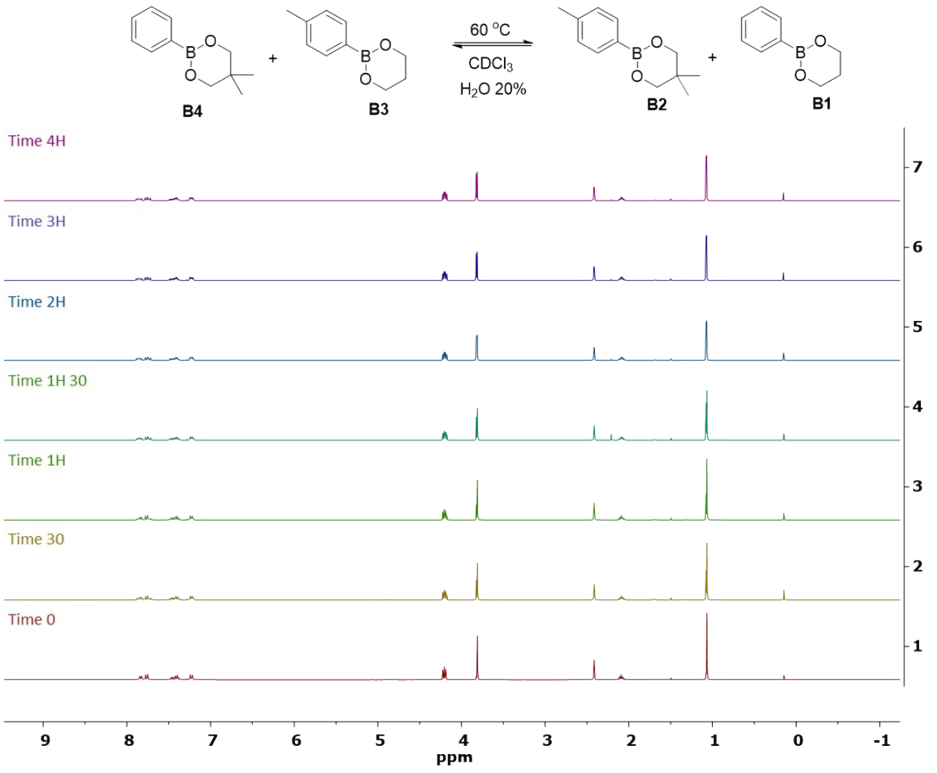

Fig. S16: Time-dependent ^{1}H NMR spectra of the reaction mixture of B4 and B3 with 20 mol% of H_2O in $CDCl_3$ at 60˚C

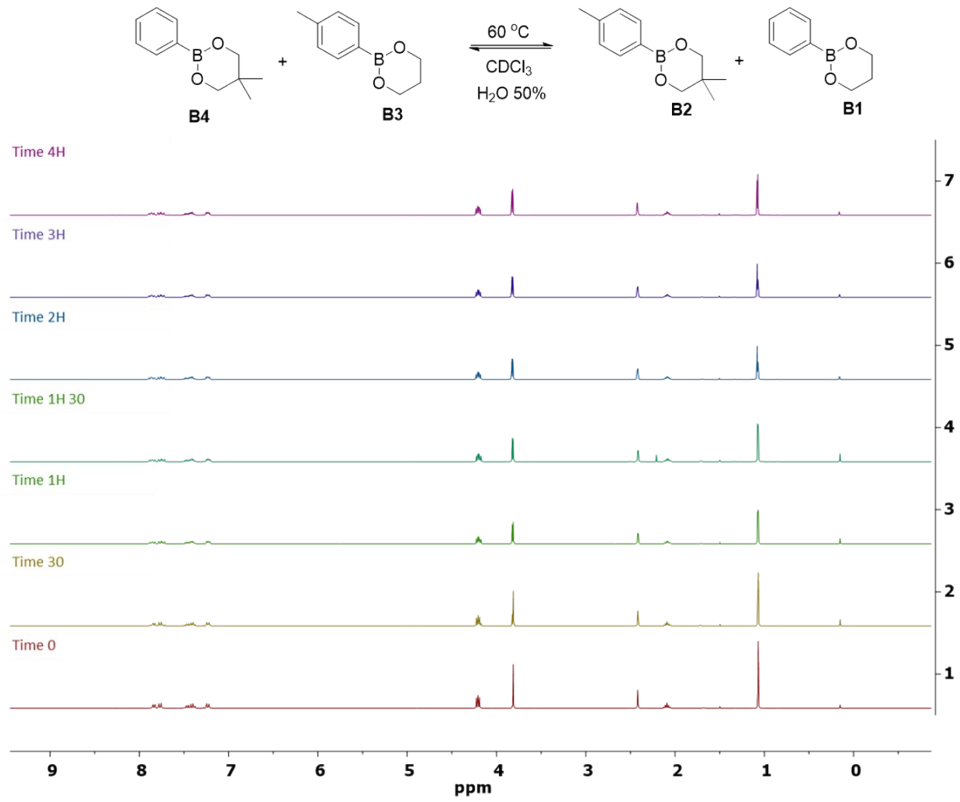

Fig. S17: Time-dependent ^{1}H NMR spectra of the reaction mixture of B4 and B3 with 50 mol% of H_2O in $CDCl_3$ at 60˚C

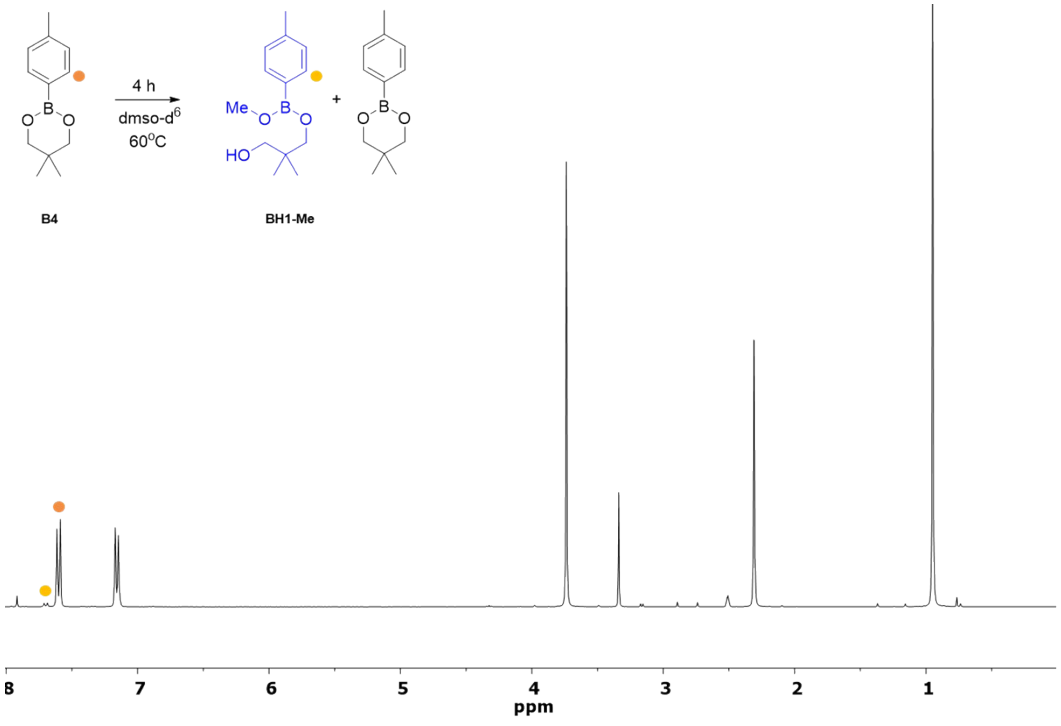

Fig. S18: ^{1}H NMR spectra of dioxaboranine B4 after 4 hours in DMSO-d^6 at 60˚C

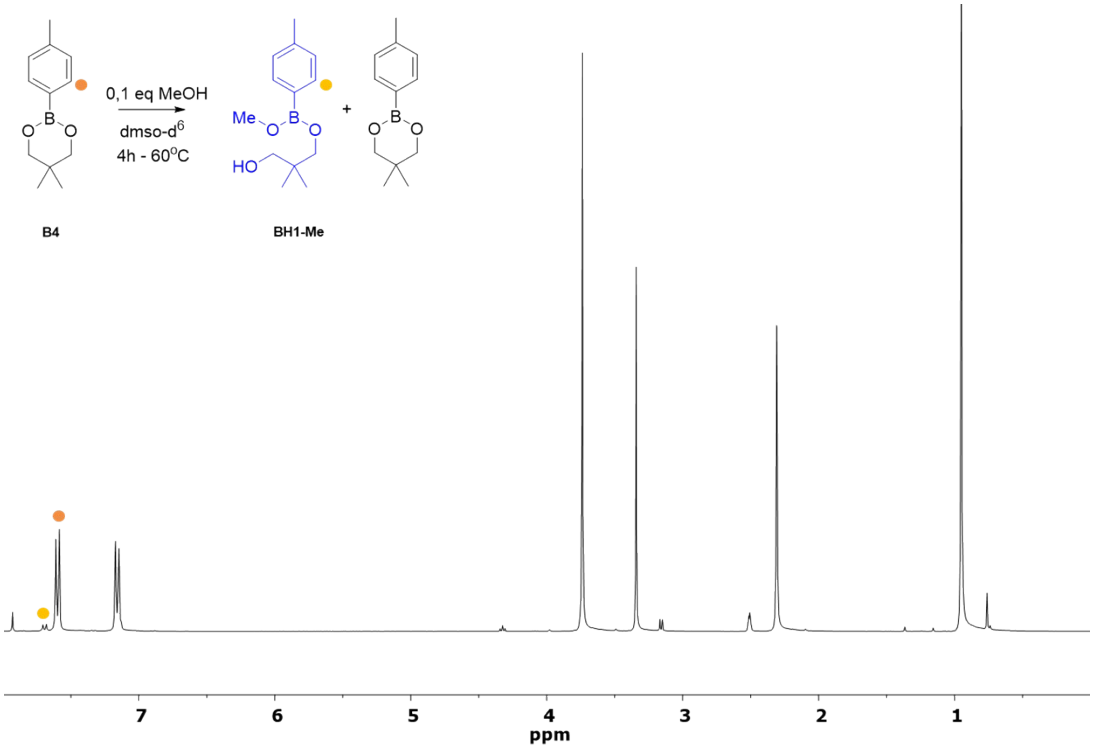

Fig. S19: ^{1}H NMR spectra of dioxaboranine B4 after 4 hours in DMSO -d^{6} at 60°C with 0.1 equivalent of MeOH

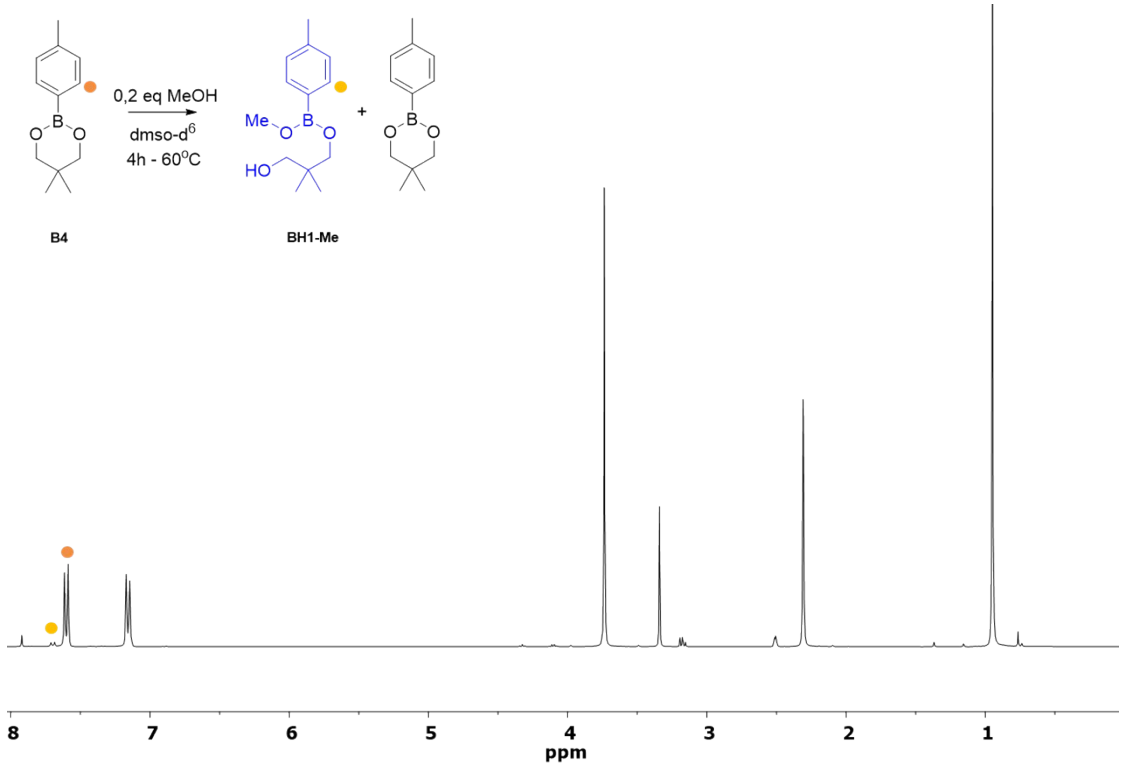

Fig. S20: ^{1}H NMR spectra of dioxaboranine B4 after 4 hours in DMSO-d^{6} at 60°C with 0.2 equivalents of MeOH

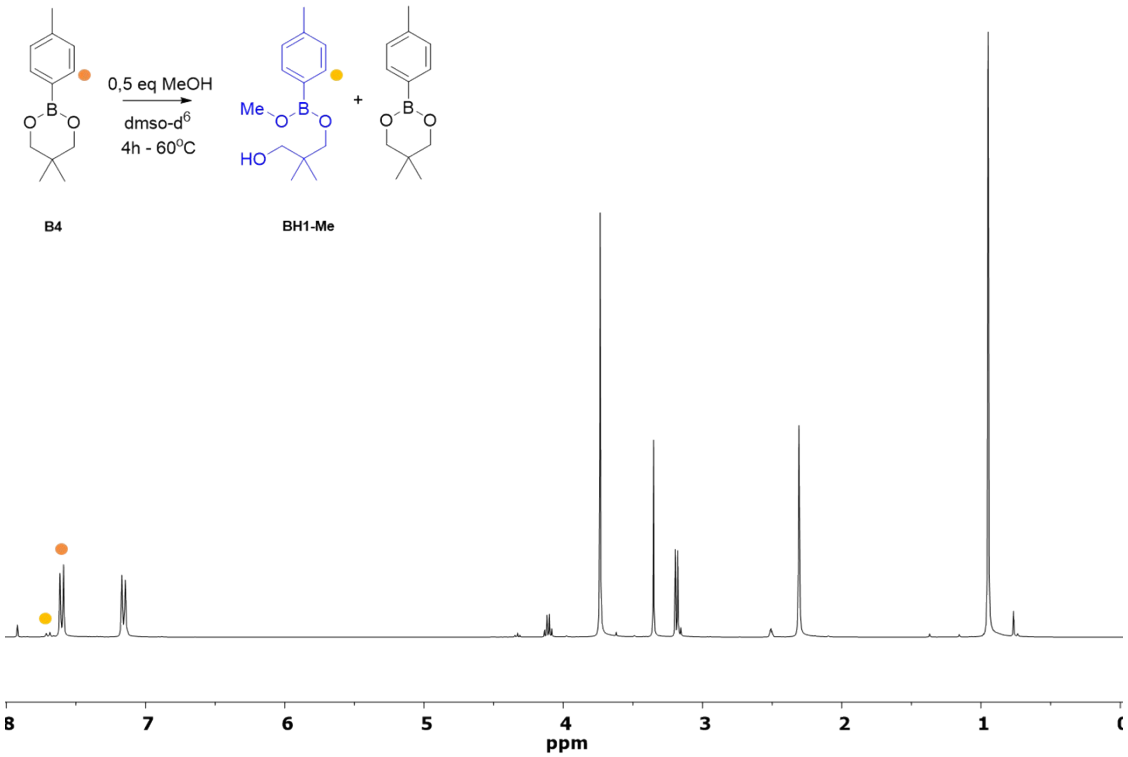

Fig. S21: ^{1}H NMR spectra of dioxaboranine B4 after 4 hours in DMSO-d^{6} at 60˚C with 0.5 equivalents of MeOH

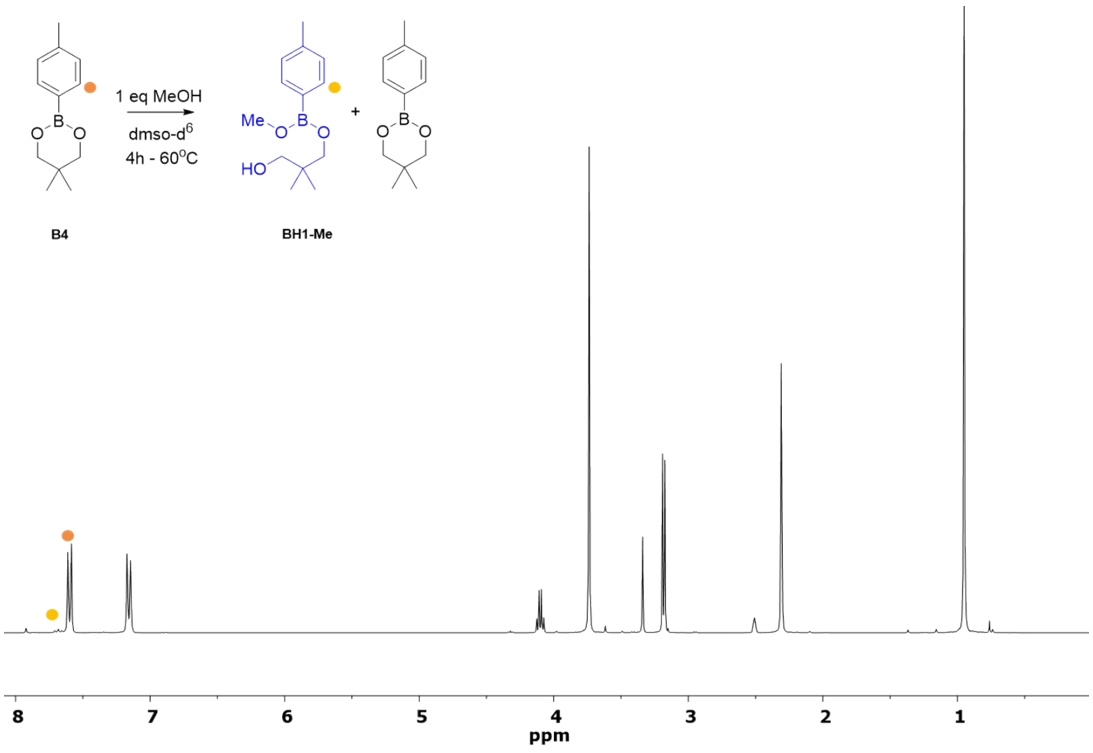

Fig. S22: ^{1}H NMR spectra of dioxaboranine B4 after 4 hours in DMSO-d^{6} at 60˚C with 1 equivalent of MeOH

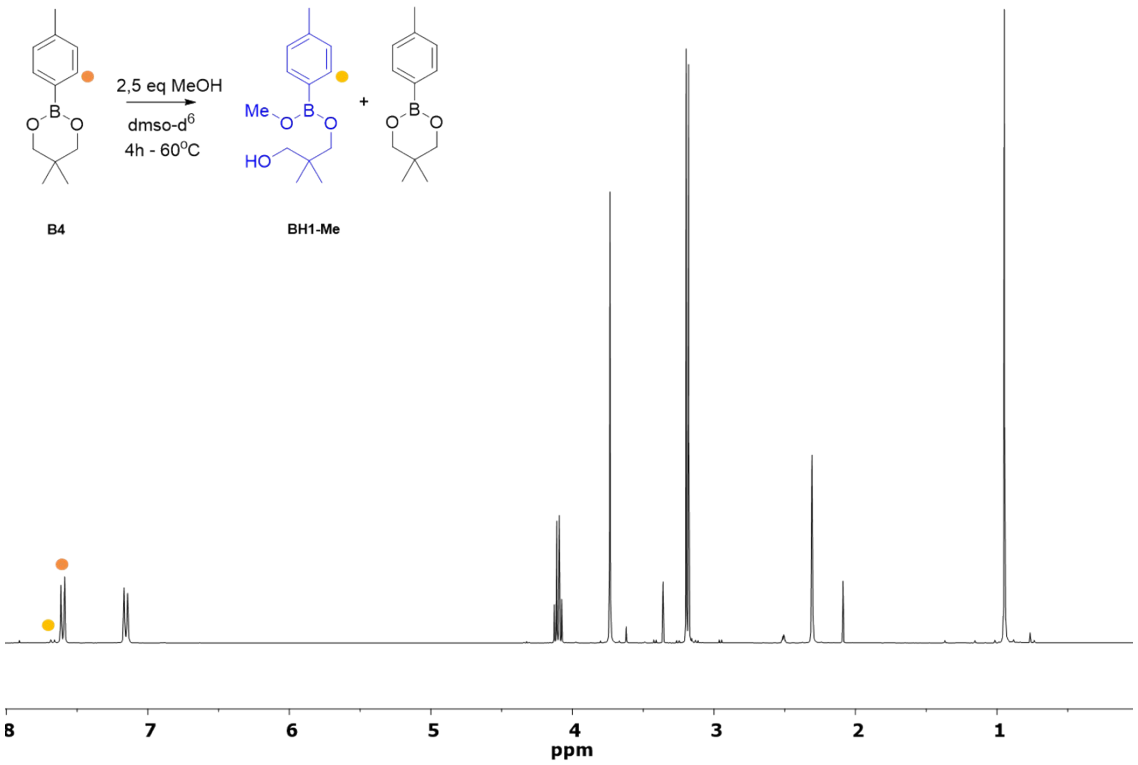

Fig. S23: ^{1}H NMR spectra of dioxaboranine B4 after 4 hours in DMSO-d^{6} at 60˚C with 2.5 equivalents of MeOH

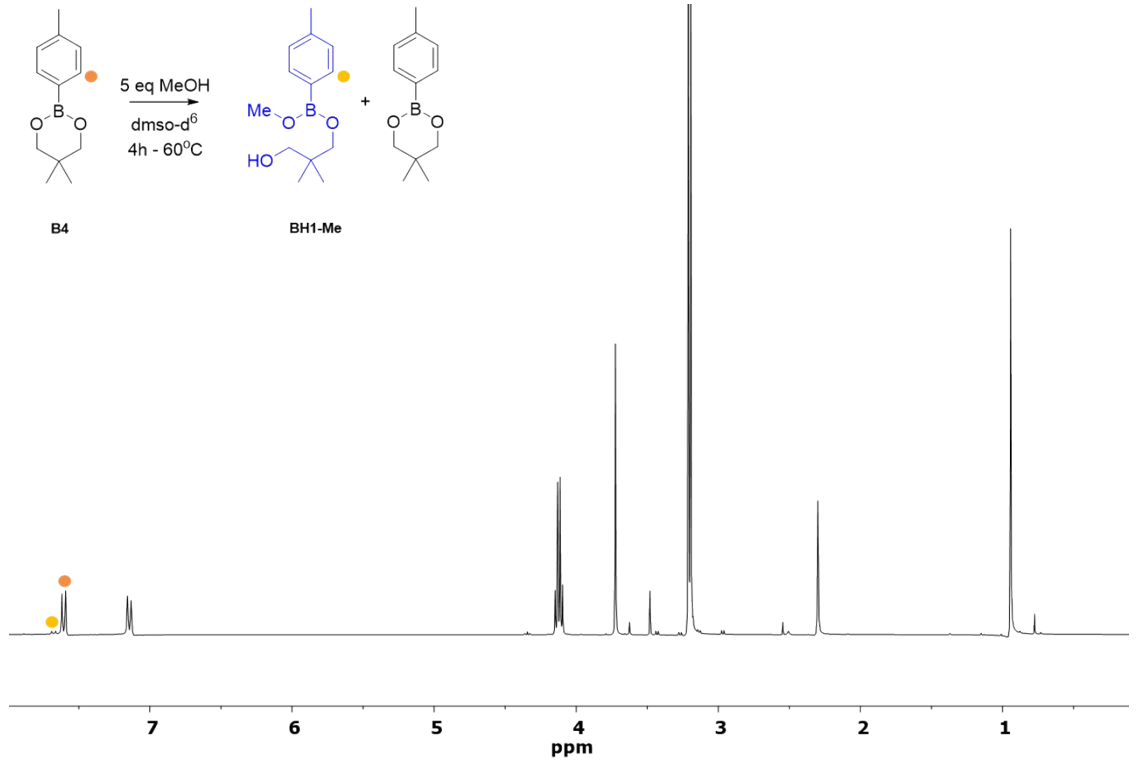

Fig. S24: ^{1}H NMR spectra of dioxaboranine B4 after 4 hours in DMSO-d^{6} at 60˚C with 5 equivalents of MeOH

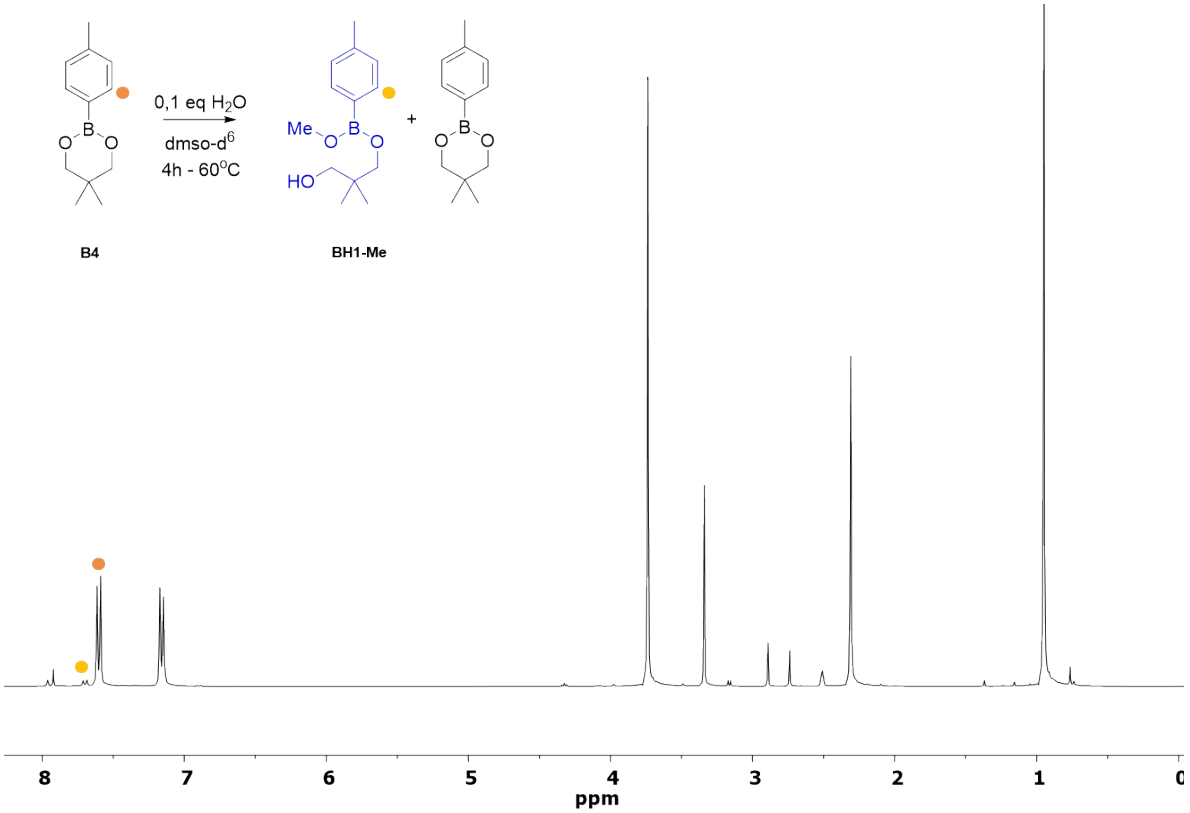

Fig. S25: ^{1}H NMR spectra of dioxaboranine B4 after 4 hours in DMSO-d^{6} at 60˚C with 0.1 equivalents of H_2O

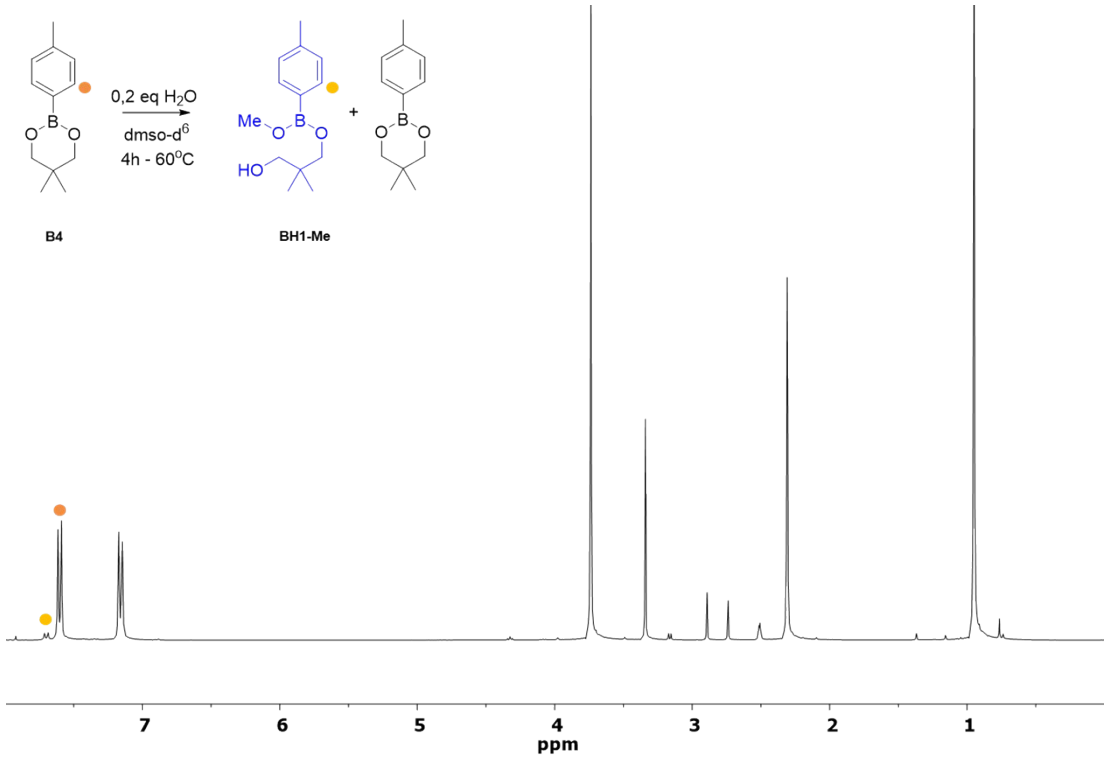

Fig. S26: ^{1}H NMR spectra of dioxaboranine B4 after 4 hours in DMSO-d^{6} at 60˚C with 0.2 equivalents of H_2O

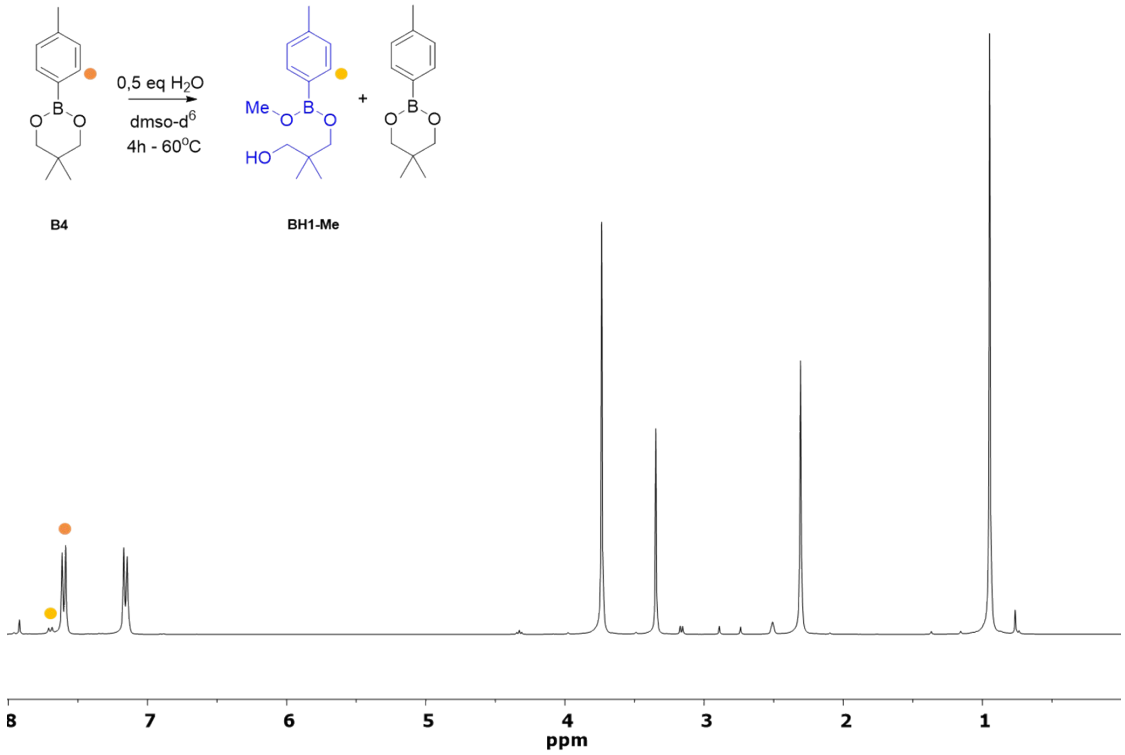

Fig. S27: ^{1}H NMR spectra of dioxaboranine B4 after 4 hours in DMSO-d^{6} at 60˚C with 0.5 equivalents of H_2O

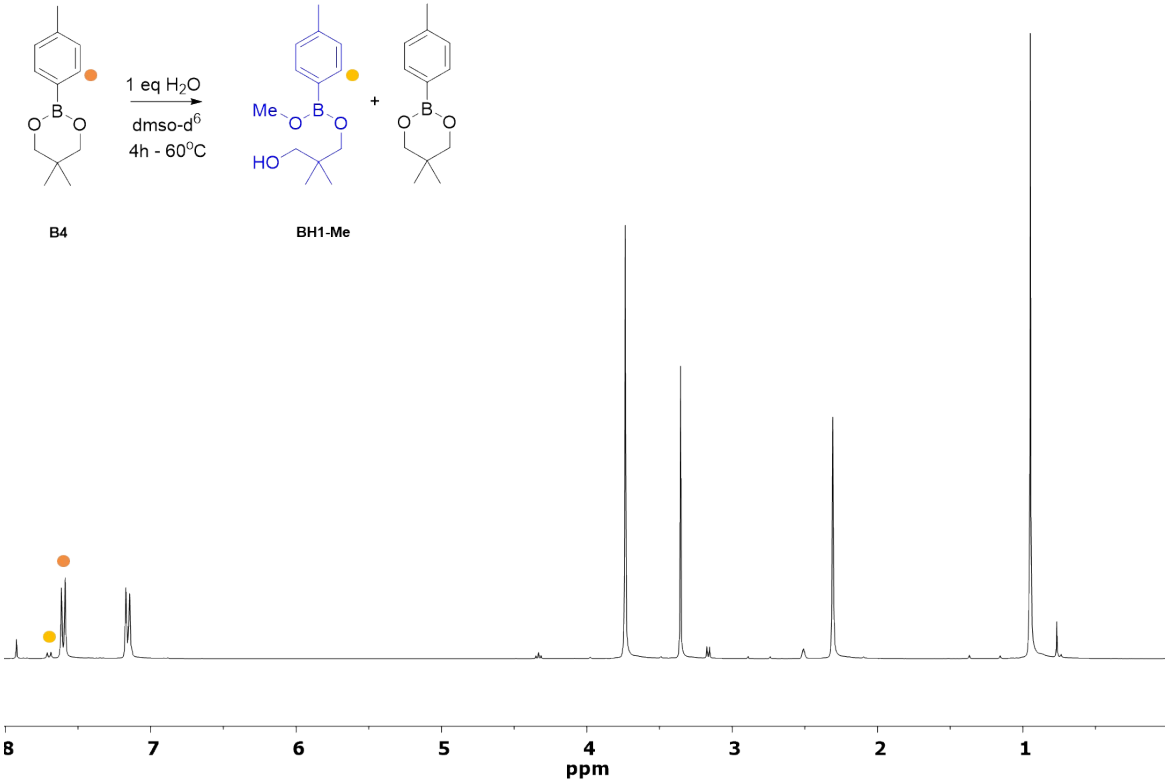

Fig. S28: ^{1}H NMR spectra of dioxaboranine B4 after 4 hours in DMSO-d^{6} at 60˚C with 1 equivalent of H_2O

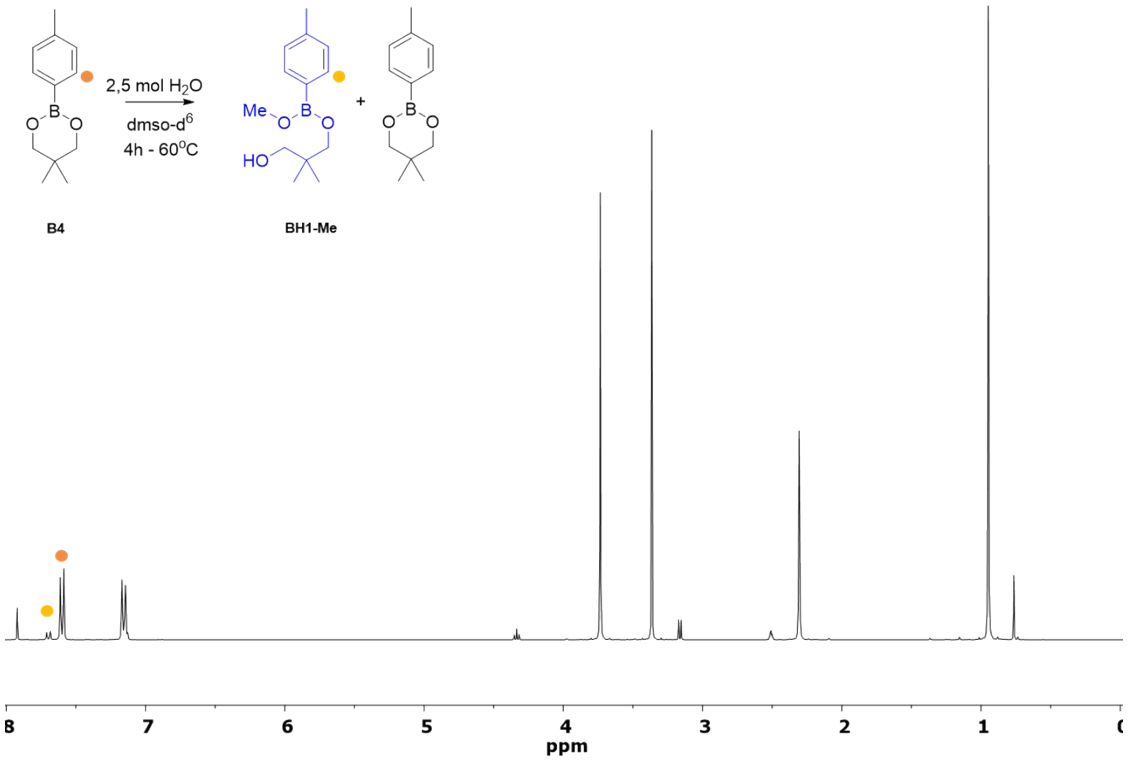

Fig. S29: ^{1}H NMR spectra of dioxaboranine B4 after 4 hours in DMSO-d^6 at 60˚C with 2.5 equivalents of H_2O

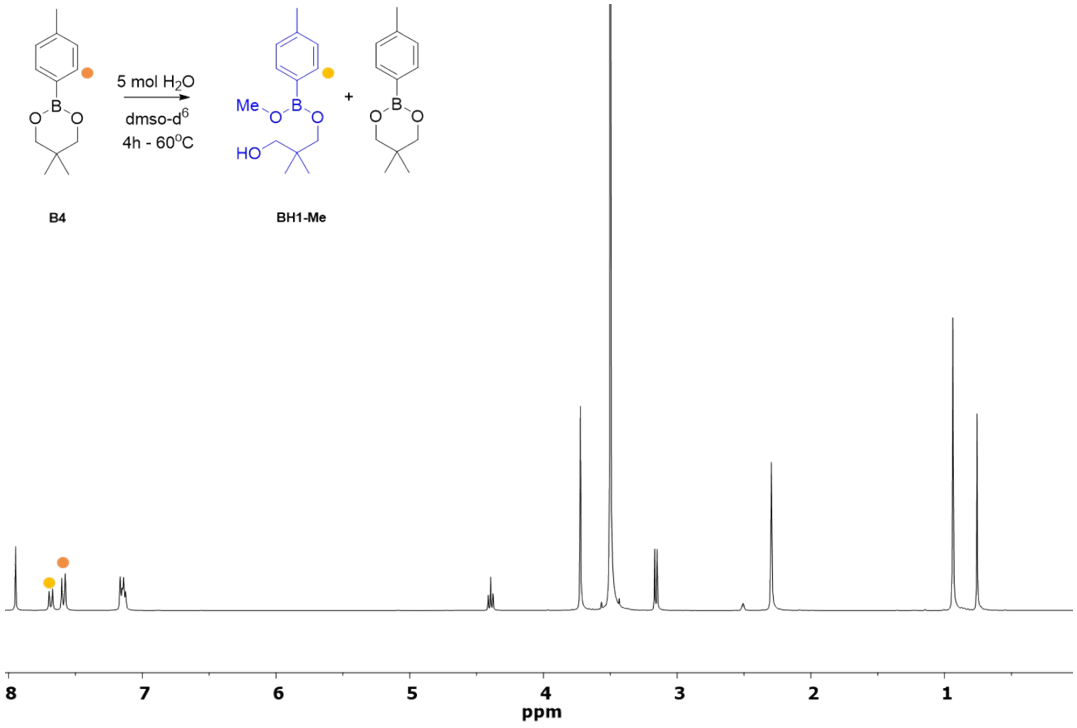

Fig. S30: ^{1}H NMR spectra of dioxaboranine B4 after 4 hours in DMSO-d^6 at 60˚C with 5 equivalents of H_2O

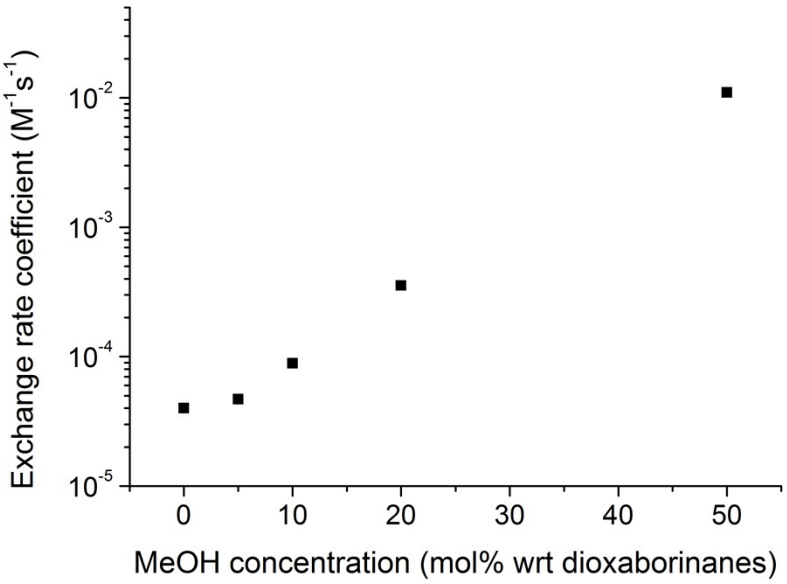

Fig. S31: Effect of concentration of MeOH on the effective rate coefficient of exchange of dioxaborinanes. The effective rate coefficients are obtained from the kinetic data shown in Figure 5 of the main manuscript by fitting the value of the rate coefficient, k_{ex}, to the rate equation $[B3] = \frac{[B3]_0}{2} + \frac{[B3]_0}{2} e^{-2[B3]_0 k_{ex} t}$ derived by assuming reversible exchange between [B3] and [B4] to give [B1] and [B2] occurs with identical rate coefficient for the forward and backward reaction.

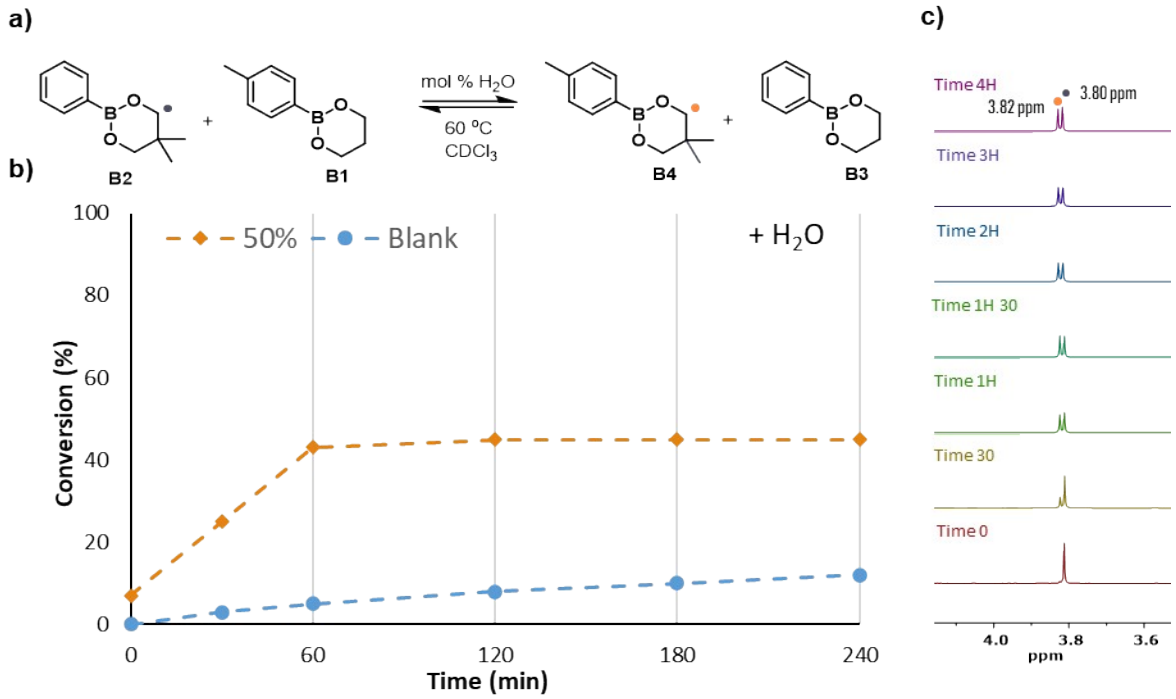

Fig. S32: Experimental kinetics between dioxaborinane B2 and B1 with H_2O as accelerator at 60°C. (a) Left panel b: kinetics of B2 + B1 in solution with H_2O. Right panel c: time-dependent 1H-NMR spectra of the reaction.

Part-III. Computational results

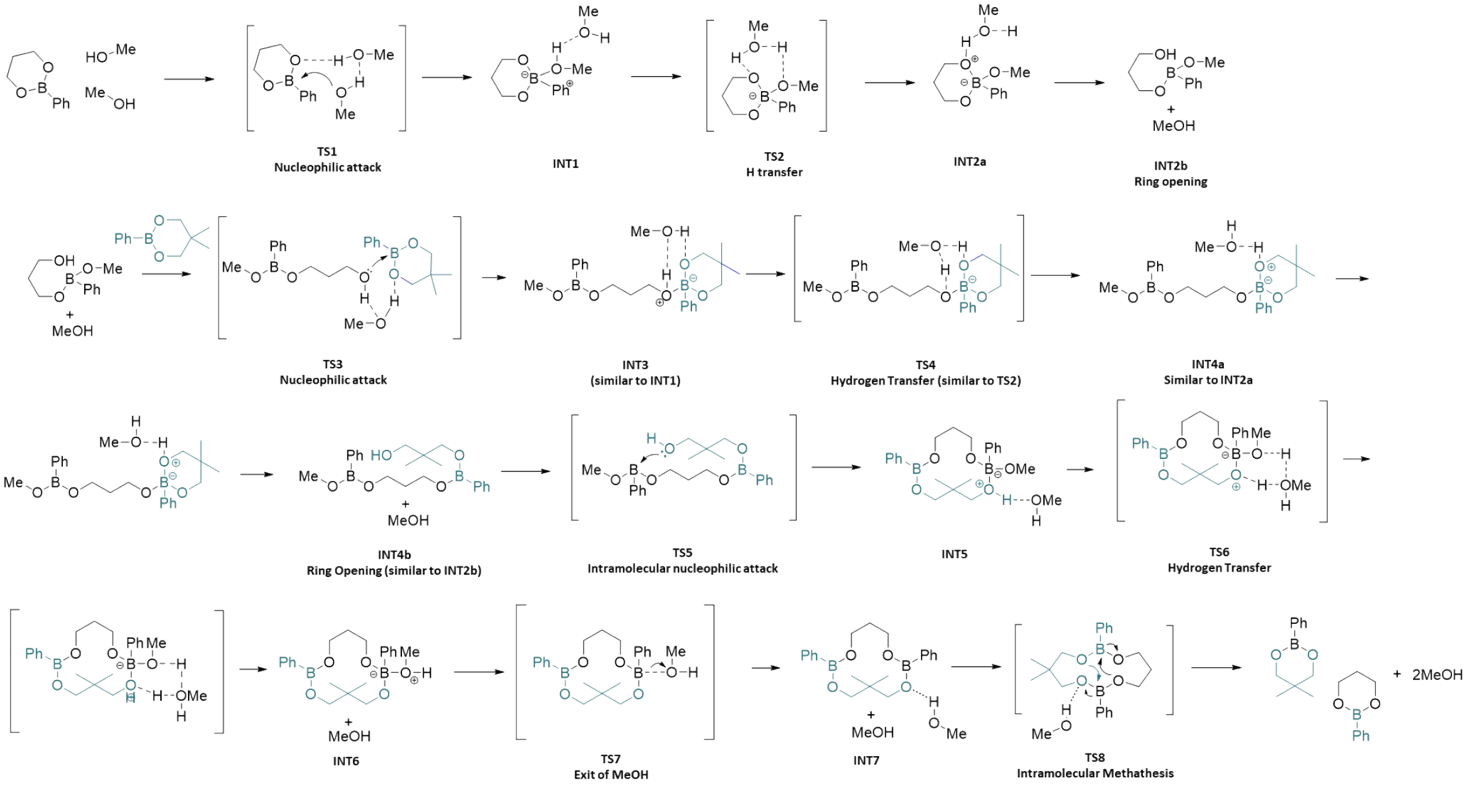

TS1 - Nucleophilic attack

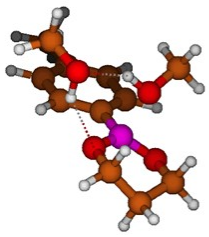

INT1

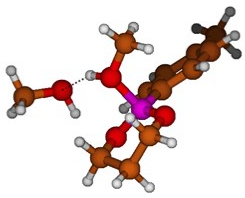

TS2 – H Transfer

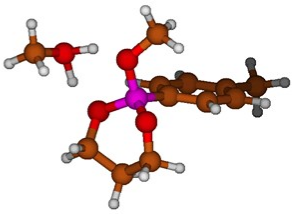

INT2B

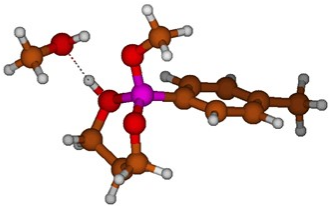

TS3 - Nucleophilic attack

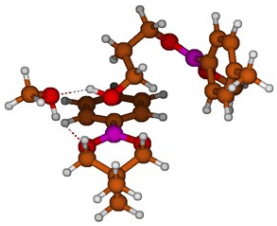

INT3

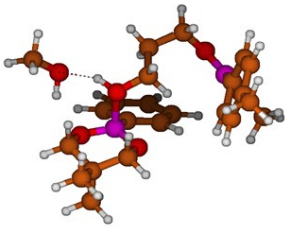

TS4 – H Transfer

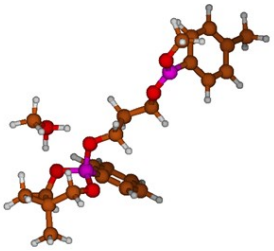

INT4

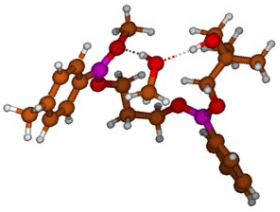

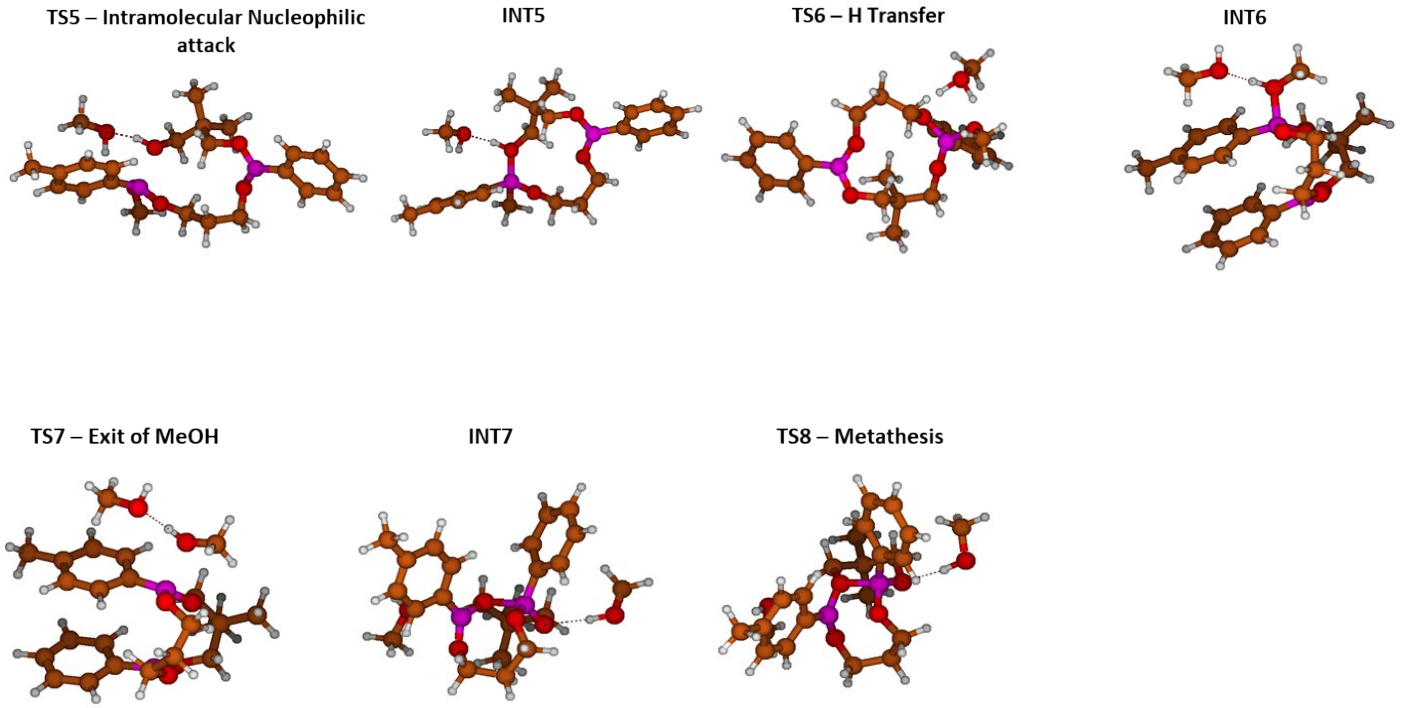

Fig. S33: Nucleophile-mediated metathesis mechanism: elucidation of the mechanistic pathway with TS and intermediates structures calculated with DFT

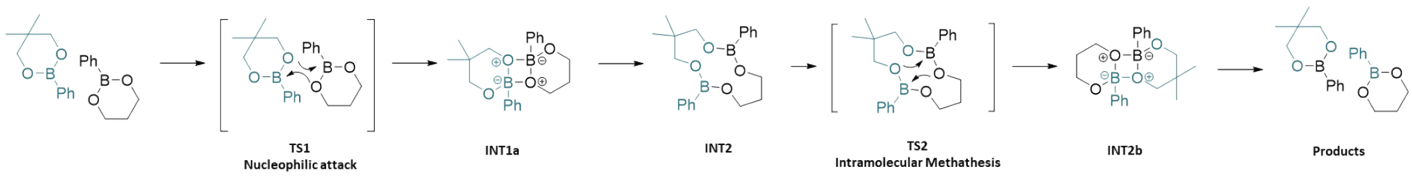

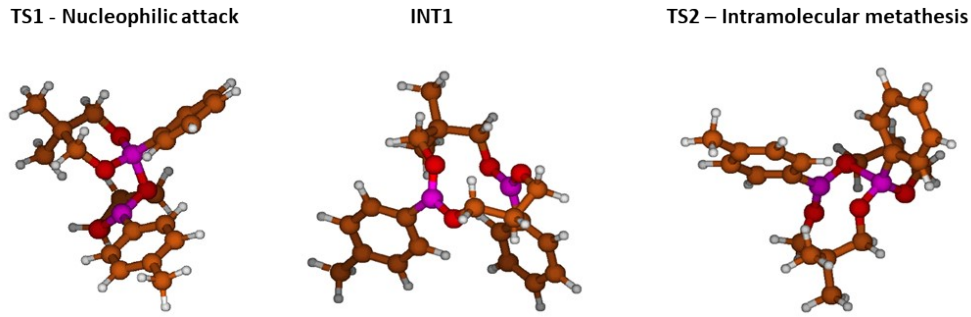

Fig. S34: Direct metathesis of dioxaboranines: elucidation of the mechanistic pathway with TS and intermediates structures obtained calculated with DFT

Part-IV. Characterization of the structure, and thermal and mechanical properties of vitrimer network prepared

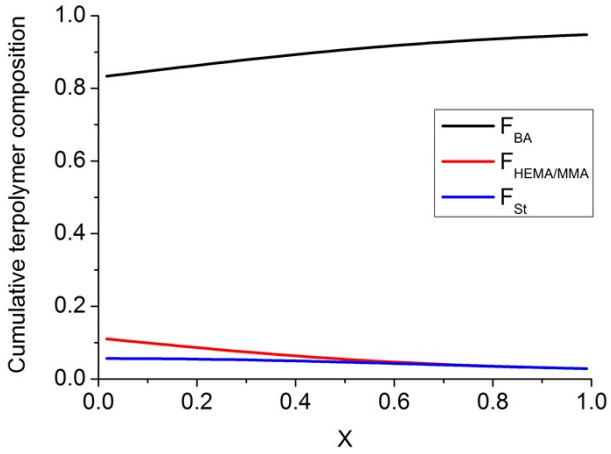

Fig. S35: Calculated cumulative terpolymer composition as a function of conversion in the terpolymerization of BA, methacrylates and styrene following formulation VT2. Note that the methacrylate component includes both HEMA and the methacrylate group of the crosslinking agent, which are assumed to react equally.

Table S1: Swelling ratio and T_g data for each formulation of vitrimer VT0, VT1 and VT2 and control crosslinked network blank.

Name	Swelling Ratio (%)	T_g (ºC)
Blank	373	-
VT0	400	-42
VT1	406	-41
VT2	371	-41

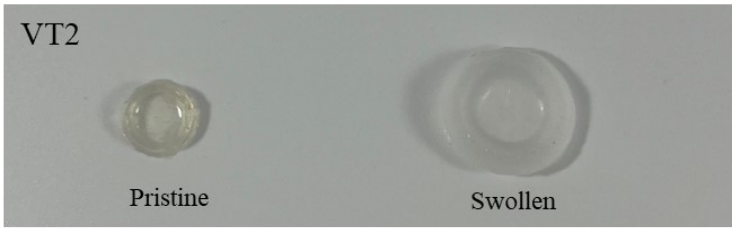

Fig. S36: Picture representing pristine VT2 (left) and the swollen in CH_2Cl_2 counterpart (right)

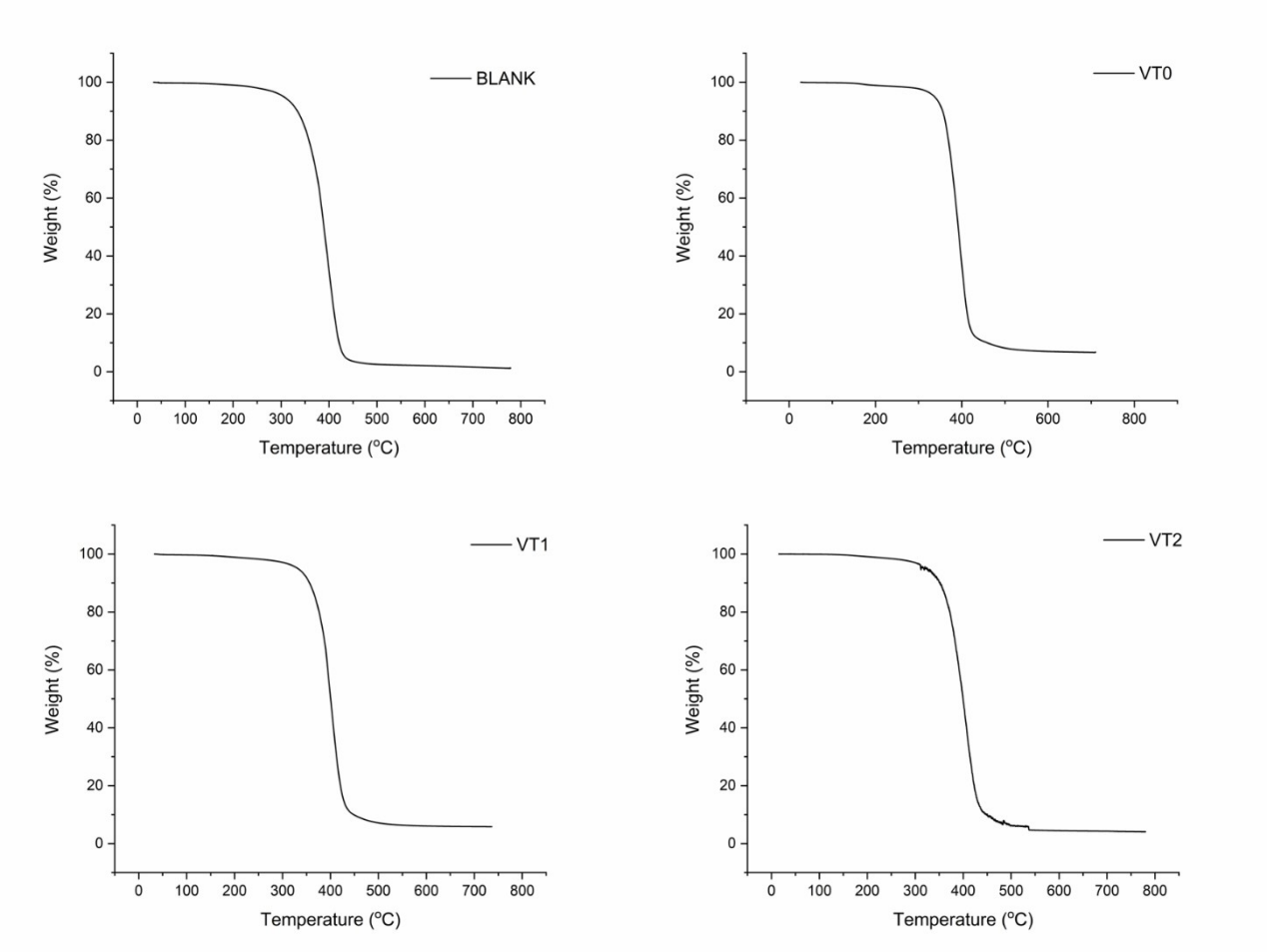

Fig. S37: Thermal gravimetric analyses of the vitrimer networks VT0, VT1 and VT2 and blank crosslinked network carried out under nitrogen atmosphere

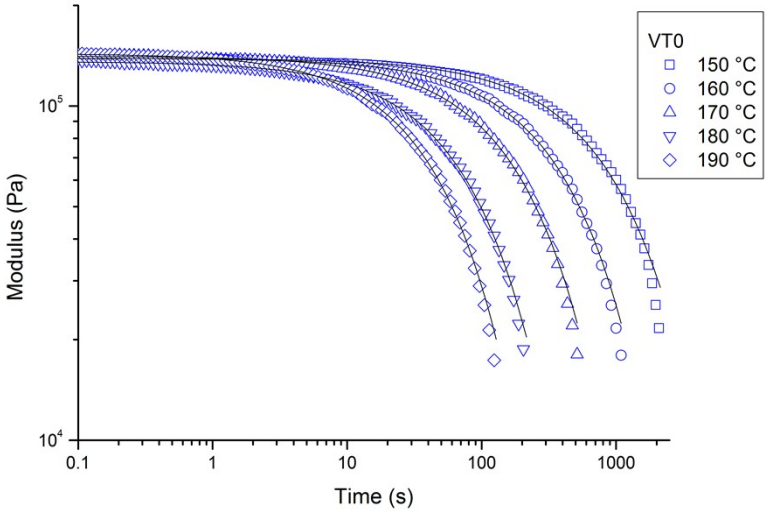

Fig. S38: Stress relaxation measurements of network VT0 carried out at various temperatures. The full lines correspond to fits of the data to a stretched exponential of the form $G(t) = G_0 e^{-\left(\frac{t}{\tau}\right)^{\beta}}$.

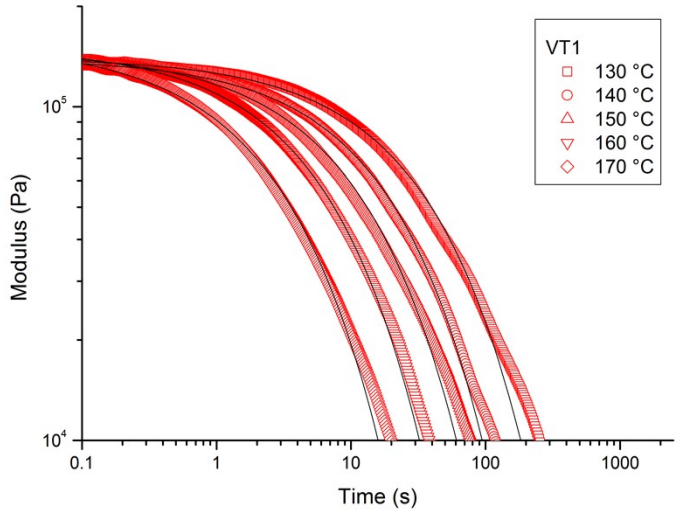

Fig. S39: Stress relaxation measurements of network VT1 carried out at various temperatures. The full lines correspond to fits of the data to a stretched exponential of the form $G(t) = G_0 e^{-\left(\frac{t}{\tau}\right)^{\beta}}$.

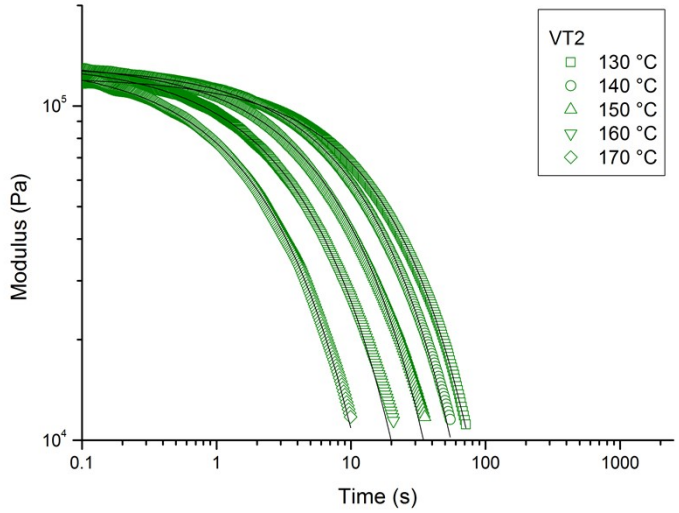

Fig. S40: Stress relaxation measurements of network VT2 carried out at various temperatures. The full lines correspond to fits of the data to a stretched exponential of the form $G(t) = G_0 e^{-\left(\frac{t}{\tau}\right)^{\beta}}$.

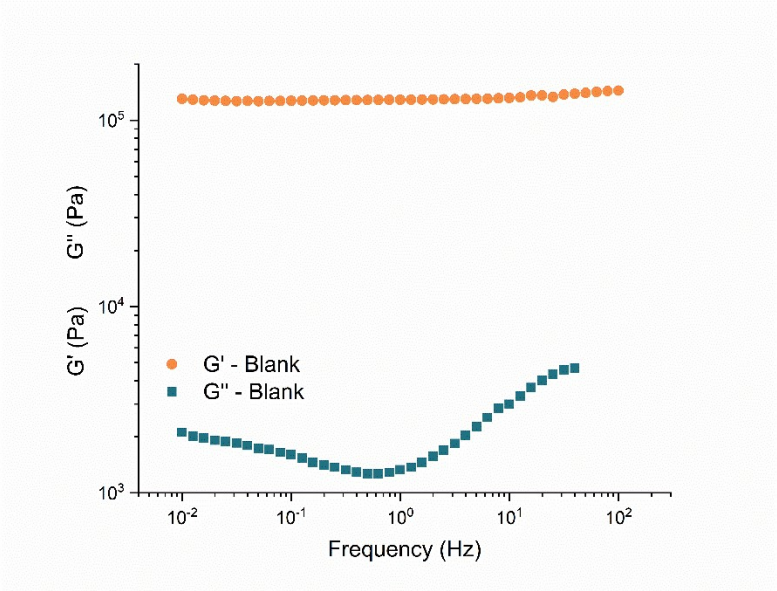

Fig. S41: Storage modulus and loss modulus of "blank" crosslinked network at 160 °C as a function of frequency.

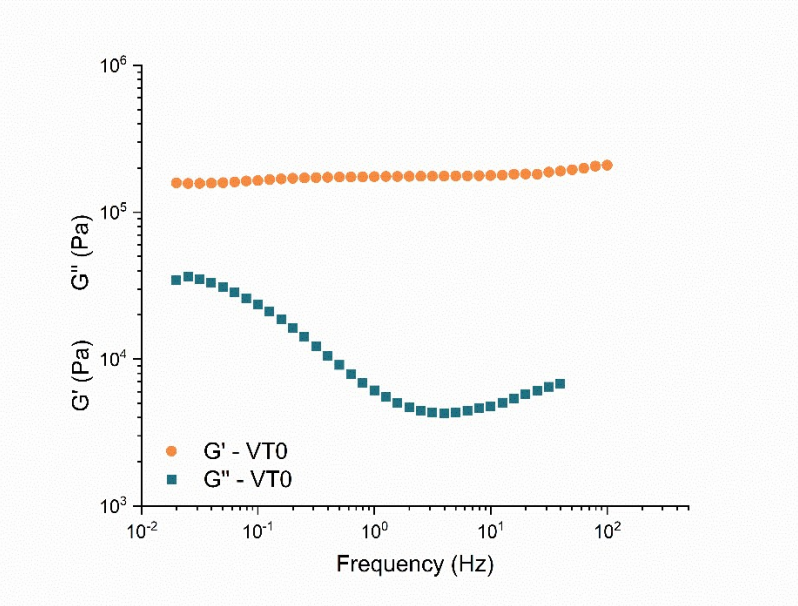

Fig. S42: Storage modulus and loss modulus of vitrimer VT0 at 160 °C as a function of frequency.

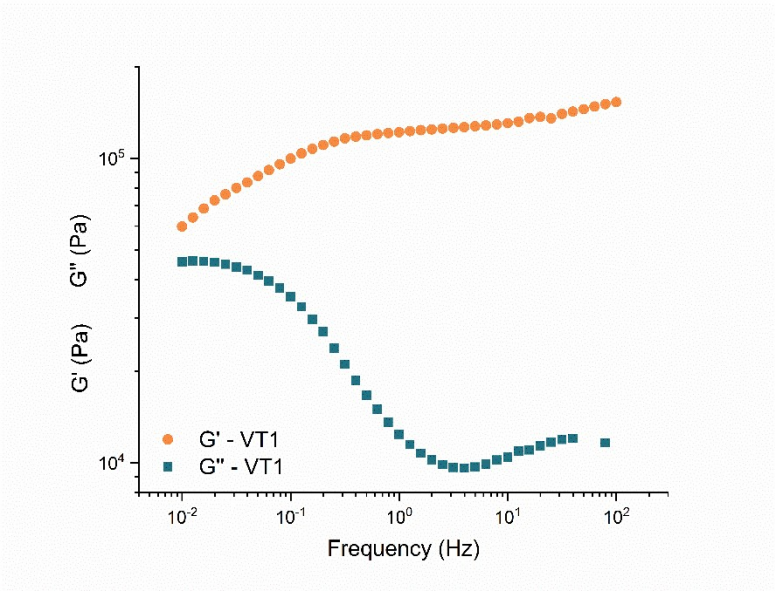

Fig. S43: Storage modulus and loss modulus of vitrimer VT1 at 160 °C as a function of frequency.

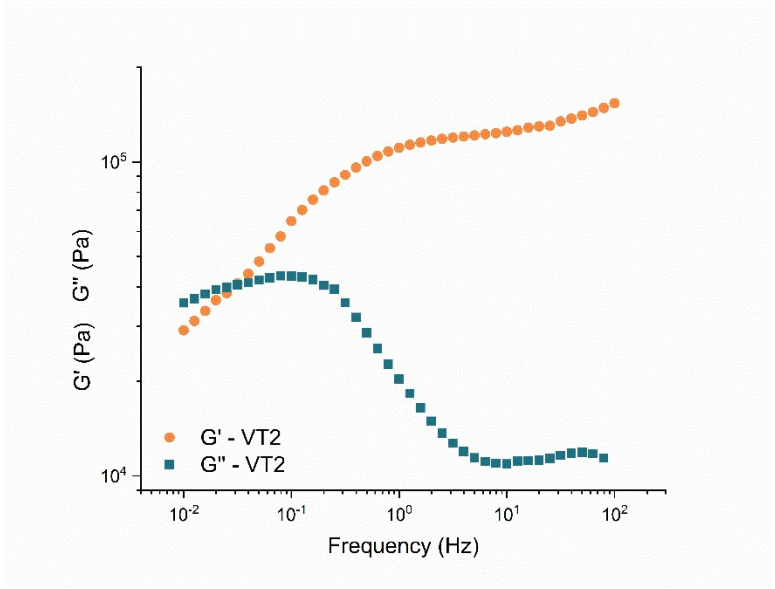

Fig. S44: Storage modulus and loss modulus of vitrimer VT2 at 160 °C as a function of frequency.

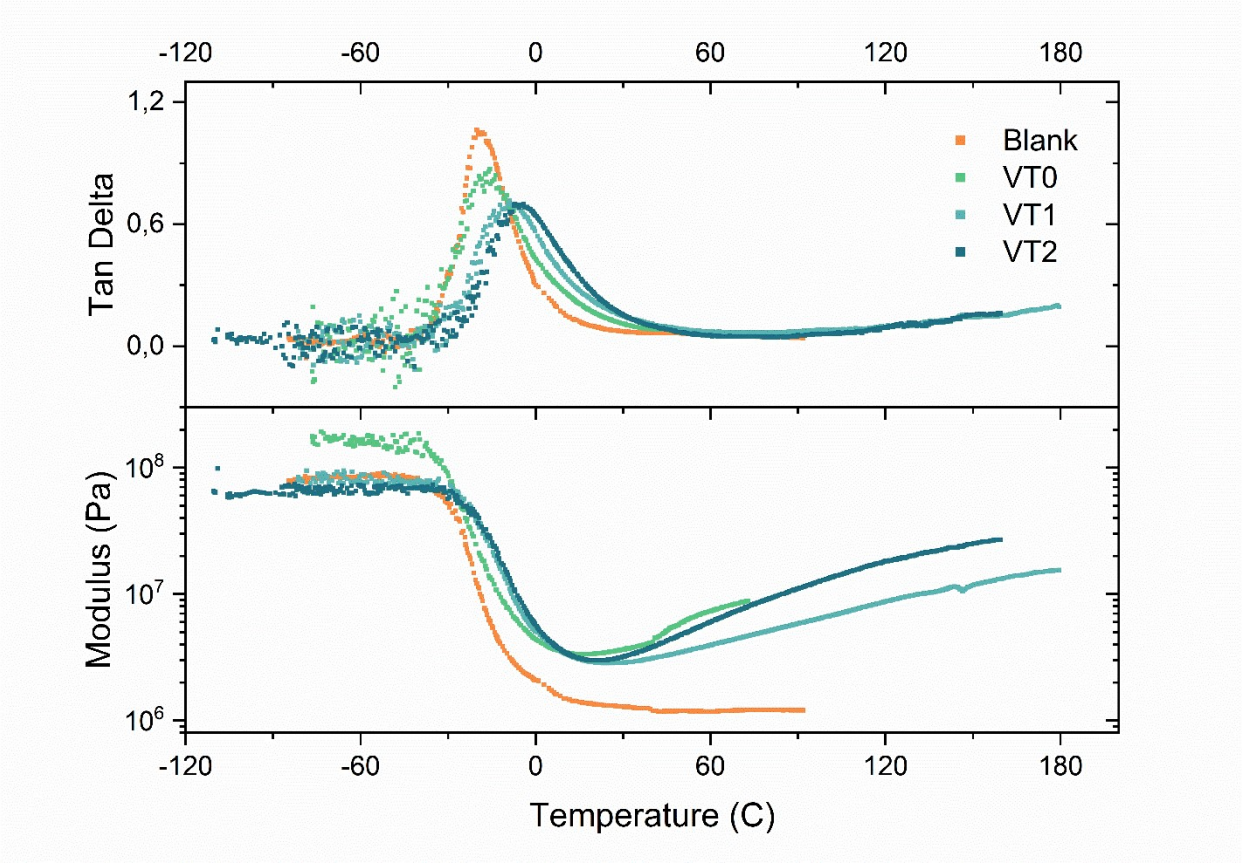

Fig. S45: Comparison of storage modulus and tan delta of control crosslinked network blank and vitrimer networks VT0, VT1 and VT2 as function of temperature. Note that the increase of the modulus above the T_g in the case of VT0, VT1 and VT2 is an artefact of the measurement due to the adhesion of the sample to the probe.

Part-VI. Reprocessing and characterization

Fig. S46: Picture representing pristine VT0 (left) and the reprocessed counterparts (right)

Fig. S47: Picture representing pristine VT1 (left) and the reprocessed counterparts (right)

Fig. S48: Picture representing pristine VT2 (left) and the reprocessed counterparts (right)

Fig. S49: Picture representing reprocessing trial of control crosslinked network “blank”

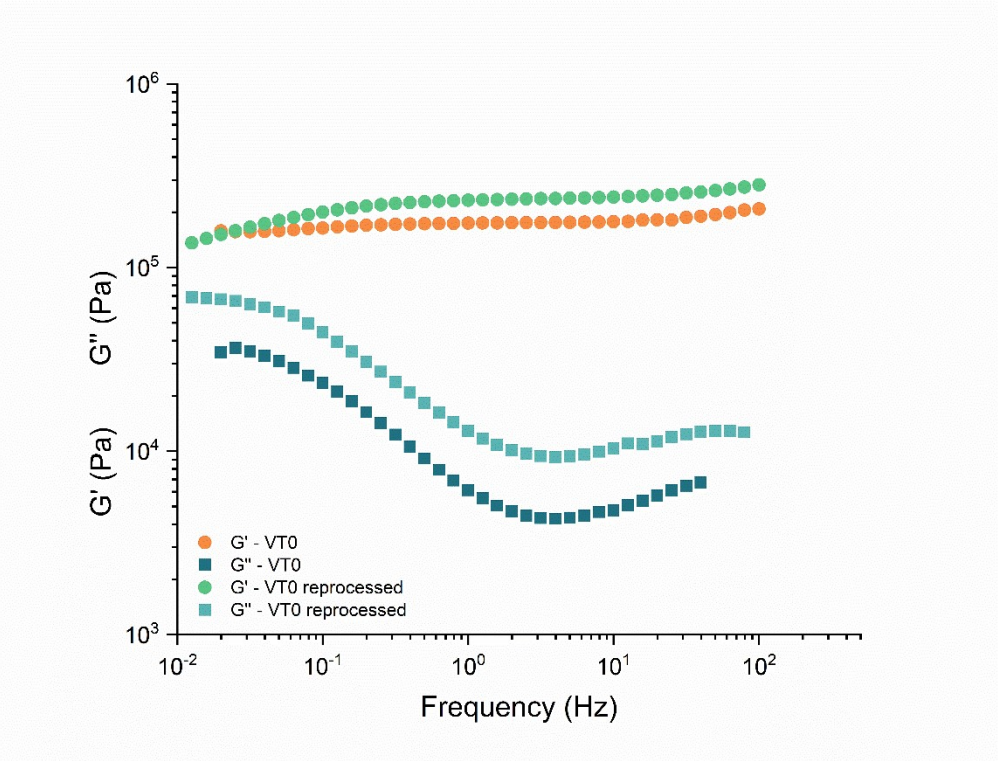

Fig. S50: Storage modulus and loss modulus of pristine and reprocessed vitrimer VT0 at 160 °C as a function of frequency.

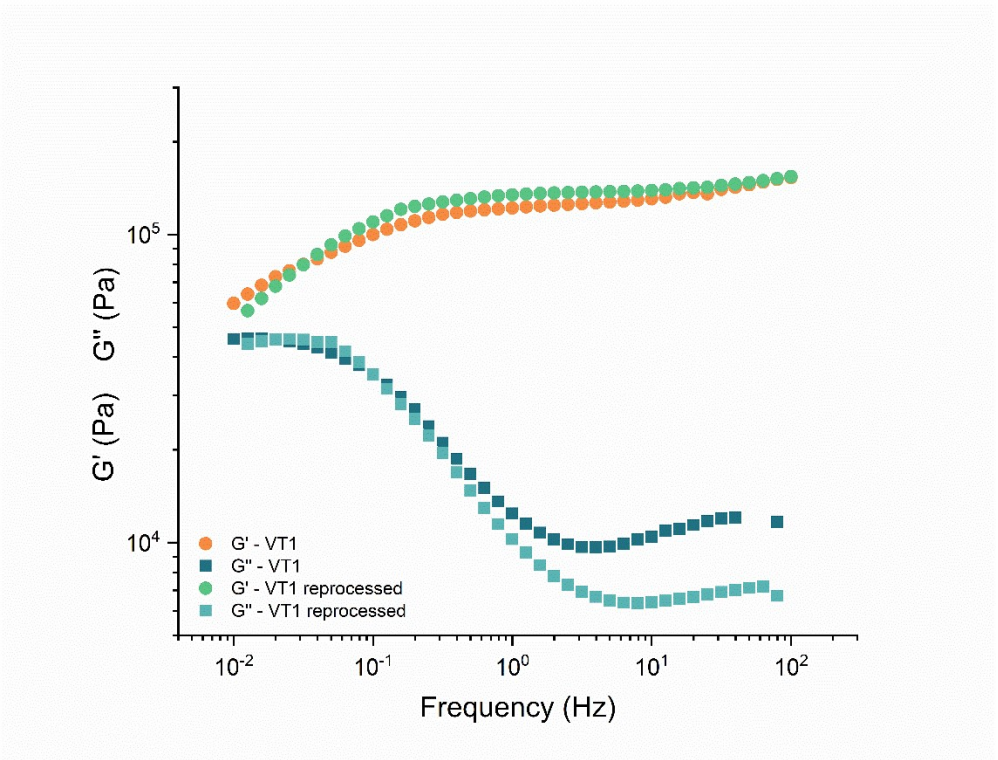

Fig. S51: Storage modulus and loss modulus of pristine and reprocessed vitrimer VT1 at 160 °C as a function of frequency.

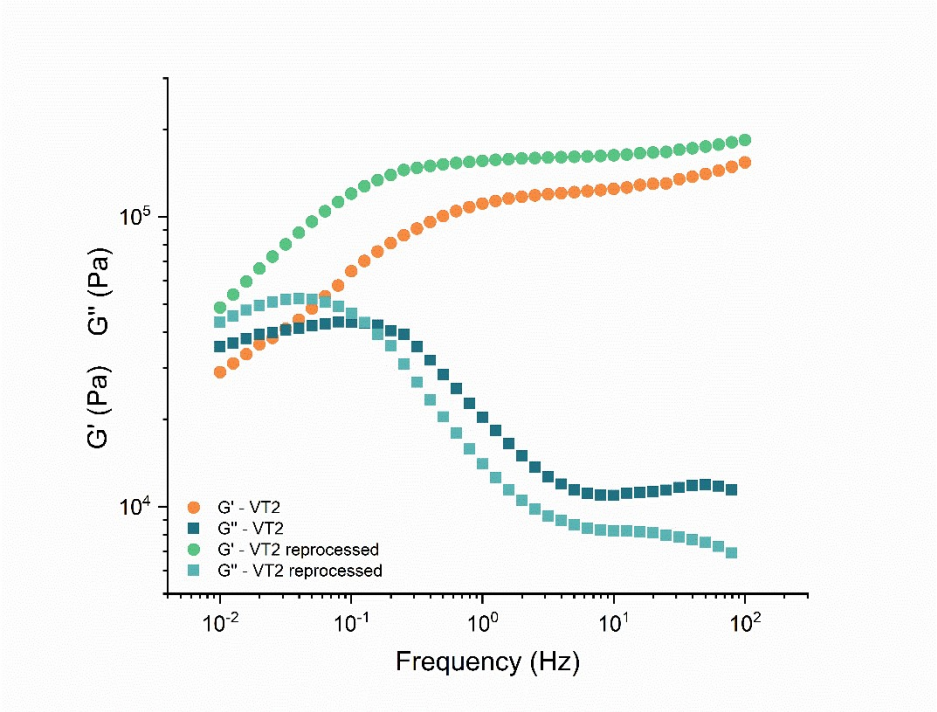

Fig. S52: Storage modulus and loss modulus of pristine and reprocessed vitrimer VT2 at 160 °C as a function of frequency.